Understanding PilB, the Type IV Pilus (T4P) Assembly ATPase

Andreas Binar Aji Sukmana

Thesis submitted to the Faculty of the Virginia Polytechnic Institute and State University

in partial fulfillment of the requirements for the degree of

MASTER OF SCIENCE

in

BIOLOGICAL SCIENCES

Zhaomin Yang, Chair

Florian D. Schubot

Michael W. Klemba

May 7, 2018

Blacksburg, Virginia

Understanding PilB, the Type IV Pilus (T4P) Assembly ATPase

Andreas B. A. Sukmana

Abstract

The type IV pilus (T4P) is a dynamic long thin fiber found on the surface of many bacterial groups. T4P is a versatile nanomachine; it plays many important roles such as for surface attachment, virulence factor, and surface motility apparatus. This research focuses on understanding the kinetics of PilB, the T4P assembly ATPase. PilB crystal structure exhibits an elongated hexamer with 2-fold symmetry indicating a symmetric rotary mechanism model. Except for its structure, the symmetric rotary mechanism of PilB has not been demonstrated experimentally. Its conformation and relatively low activity constrained previous *in vitro* studies of PilB. This study identified PilB from thermophilic organism *Chloracidobacterium thermophilum* (*Ct*) to be a model for *in vitro* studies. An active *Ct*PilB was successfully expressed and purified as a hexamer. Malachite green phosphate assay was used to examine *Ct*PilB ATPase activity. The examination indicated that *Ct*PilB is a robust ATPase with a complex kinetics profile. The profile has a stepwise incline in ATPase activity as a function of [ATP] that led to a decline in higher [ATP]. The decline was confirmed to be a substrate inhibition by the enzyme-coupled assay. As for the incline, the detailed mechanism is still less clear to explain the multiphasic profile. The overall incline did not conform with classical Michaelis-Menten kinetic but the first part of the incline was shown to conform with Michaelis-Menten kinetics. The complex kinetics profile of PilB is consistent with the symmetric rotary mechanism of catalysis.

Understanding PilB, the Type IV Pilus (T4P) Assembly ATPase

Andreas B. A. Sukmana

General Audience Abstract

This research was conducted to understand type IV pilus (T4P), a hair-like structure found on the surface of many bacteria groups. T4P is a versatile structure; it plays many vital roles in bacterial life such as in surface motility, surface attachment, gene transfer, and virulence factor. Pilus is a dynamic polymer composed of many small pilin proteins that can be assembled or disassembled. Structurally, pilus is supported by machinery that helps to extend and retract pilus by adding or removing pilin proteins. At the core of the machinery, two different proteins are responsible to power the assemble and disassemble process by converting the chemical energy in ATP into mechanical energy. This study focuses on the protein that powers pilus assembly, PilB. Understanding PilB will be very beneficial in elucidating how the strongest biological motor work in action. The structure of PilB was determined to be a hexamer consist of six identical copies of the same protein forming a ring structure with 2-fold symmetry. This structure suggests that PilB works using symmetric rotary mechanism. Previous studies of PilB have not been productive because the purified PilB did not behave well during the assay. In this study, PilB from *Chloracidobacterium thermophilum* (*Ct*PilB) was determined to be a reasonable model for the study. *Ct*PilB was successfully purified and it was identified to have a robust activity outside the cell allowing for further biochemistry studies. The profile of CtPilB kinetics was unique and it did not conform with the classical kinetic profile. The analysis of the profile suggests that *Ct*PilB exhibit a complex mechanism in hydrolyzing ATP.

Acknowledgments

I would like first to thank my advisor, Dr. Zhaomin Yang, for all the guidance and continuous support. I would also like to thank my committee members, Dr. Florian Schubot and Dr. Michael Klemba for their invaluable contribution throughout my study. I am also grateful to the present and past members of the Yang lab and Schubot lab (Qi Zhang, Manisha Shrestha, Jordan Mancl, Dawn Wright, Stephanie Franco, Keane Dye, and Kristine Yarnoff). Thank you all for the great conversations, many encouragements, and many other things. I would like to express my gratitude to my home institution, Satya Wacana Christian University, for all the support. Last but not least, I would like to thank Fulbright for their scholarship that supports me for the first two years of my study and allowed me to fulfill my dream to study abroad.

Table of Contents

List of Figures

Chapter 1

Literature Review

T4P are prevalent and are an important structure

The Type IV Pili (T4P) are thin, flexible, extracellular appendages prevalent across nearly all phyla of prokaryotes domain (1,2) (Fig. 1A). Evolutionary, the T4P has a high degree of similarity compared to the Type II Secretion System (T2SS). Both the T4P and the T2SS share many conserved homolog proteins (3). Some information from the T2SS is often being used to shed light on studying the T4P as a comparable model system (4). One cell can have up to 10 pili and they usually are located at the cell's' pole (5). These structures play diverse essential roles such as surface attachment, biofilm formation, natural transformation, and surface motility (6-8). The fibers are composed of helically polymerized pilin monomer and are around 5- to 8-nm in diameter with the length up to several micrometers. The T4P are dynamic structures that undergo cycles of extension, attachment, and retraction (9,10). The extension of pili is facilitated by the polymerization/addition of pilin protein from the base of the growing pili. The extrusion of the extending pili from the cell envelope is then followed by the attachment of the pili's tip on a surface. After the attachment, the pili will be retracted by disassembling pilin protein starting from their base resulting in a forward movement in the direction of the cell's long axis (11).

The T4P of the Gram-negative bacteria i known to be the strongest biological motor currently known. The strong retraction power of the T4P supports the surface motility by pulling the cells forward with the velocity of few tenths of a micrometer per second. The retraction power of the T4P from *Neisseria gonorrhoeae* and *Myxococcus xanthus* produce stall force of around 100 pN and 150 pN respectively (12,13). Those retraction powers exceed previously studied

biological motors such as phage Φ29 packaging ATPase, flagellin, and kinesin at 60 pN, 7.5 pN, and 5 pN (14-16). The extension and retraction were made possible by the proteins building the T4P machinery complex which spans across the envelope of the bacterial cell (Fig. 1B) (17).

The T4P molecular machinery system

In the T4P system, pilus is composed of the polymerization of mature pilin protein (1). Major pilin subunit PilA is synthesized as pre-protein with an N-terminal signal peptide. Endopeptidase PilD process preprotein PilA by removing the signal peptide and anchoring mature PilA in the inner membrane (18). Pilus protrudes across the OM through a channel created by PilQ oligomer which is suggested to consist of 12 to 15 subunits (19,20). PilQ oligomerization is suggested to be stimulated by pilotin protein Tgl and stabilized by peptidoglycan binding protein TsaP (21). TsaP secures the OM secretin complex PilQ to the peptidoglycan and helps to connect it to the alignment complex. The alignment complex connects to the secretin complex via inner membrane lipoprotein PilP. The C-terminus of PilP is suggested to interact with PilQ while its periplasmic domain interacts with integral IM PilN/O heterodimer. The cytoplasmic region of PilN is suggested to recruit cytoplasmic alignment protein PilM. Assembled PilM ring at the base of the T4P is thought to assist the formation of motor complex PilC and PilB or PilT. Polytopic inner membrane protein PilC is responsible for assembling pilin into growing pilus during extension or disassemble pilin from pilus fiber during retraction (17). These two distinct processes are powered by ATP hydrolysis conducted by cytoplasmic protein PilB the assembly ATPase and PilT the disassembly ATPase (22).
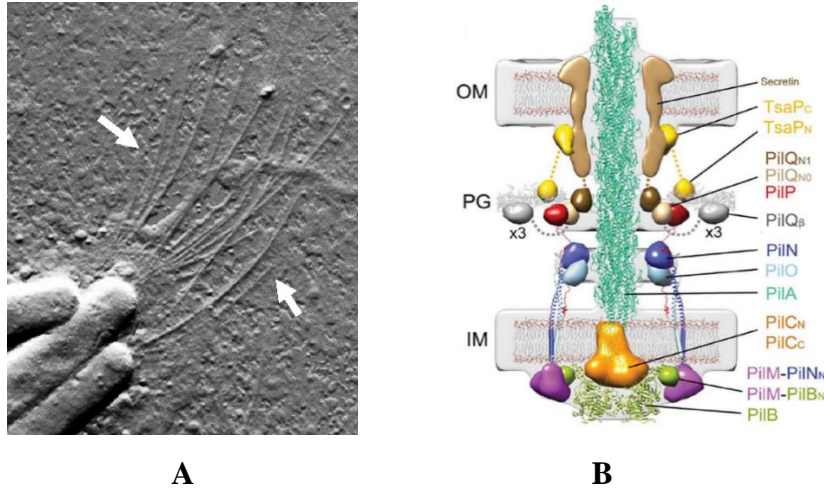
Figure 1-1. The T4P structures. (A) *Myxococcus xanthus* polar pili observed under atomic force microscope (23). (B) A model of *M. xanthus* T4P machinery is showing the component proteins spanning across the inner membrane and outer membrane (17). Used under fair use, 2018.

Although most if not all protein components of the T4P have been identified, the mechanism of how pilus is being assembled or disassembled is not yet fully elucidated. More specifically, how the chemical energy from ATP can be transformed into mechanical movement through protein-protein interaction powers the T4P dynamics.

PilB is a T4P motor protein that powers pilus assembly

The T4P assembly motor ATPase PilB facilitates the process of pilus extension. Structurally, PilB is a member of AAA+ (ATPases Associated with diverse cellular activities) superfamily (24,25). AAA+ proteins perform a wide array of cellular function such as protein degradation, DNA uptake, signal transduction as well as cell motility (26). As an AAA+ ATPase, PilB exhibits conserved Walker A and Walker B motif that are essential for the ATP hydrolysis (27,28). The force generated from ATP hydrolysis is then coupled to induce conformational changes that further translated into a mechanical force. Proteins in this group are usually active as a ring-shaped hexamer (26).

3
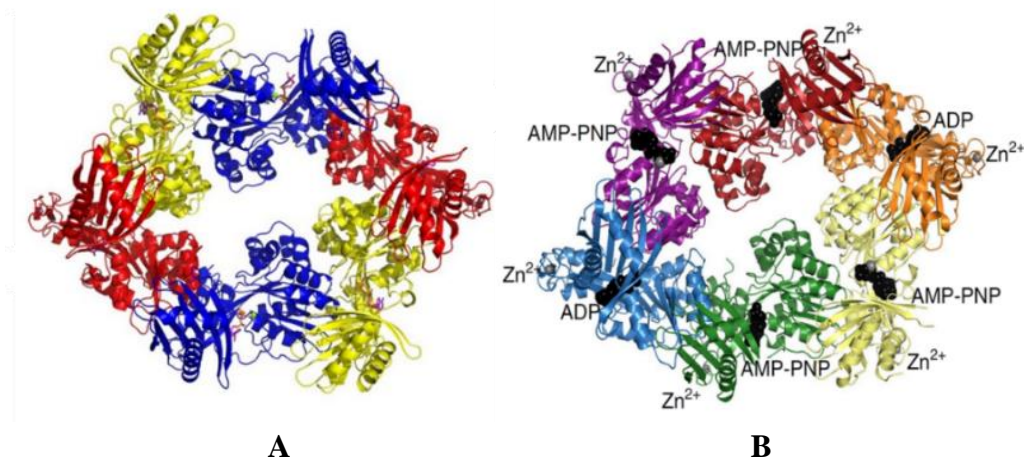
Figure 1-2. Crystal structure of core ATPase hexameric *Tt*PilB (A) and *Gm*PilB (B) showing an elongated ring. Two protomers with high affinity for ATP binding and are in the closed conformation facing each other in both TtPilB (blue colored protomers) and *Gm*PilB (red and green colored protomers) (29,30). Used under fair use, 2018.

The study involving PilB crystal structure from *Thermus thermophilus* (*Tt*PilB) and *Geobacter metallireducens* (*Gm*PilB) revealed that PilB forms hexamer (Fig. 2) (29,30). The structural movement of PilB is possible by the presence of flexible linker between the N-terminal domain (NTD) and C-terminal domain (CTD). The nucleotide binding pocket of PilB is in the interface between NTD and CTD, in agreement with the common AAA+ characteristic (30). In the CTD, PilB also has coordinated metal domain where four cysteine residues coordinate one Zn^{2+} ion which is important for stabilizing the hexamer complex. The NTD of one protomer is connected to the CTD from adjacent protomer forming a rigid body (29).

Despite the importance of PilB in supporting such a processive system, there have been no biochemical studies to support the rotary mechanisms of catalysis by PilB. The limiting factor appears to be the low ATPase activity of PilB from *M. xanthus* and *Pseudomonas aeruginosa*, the two model systems for the studies of T4P-mediate bacterial motility. *In vitro* study of purified monomer PilB displays that they had a relatively low ATPase activity ranging from 2.9 to 10.8

nmol Pi/mg PilB/minute. This low activity does not seem to support T4P as the strongest biological.

Moreover, purified PilB from *M. xanthus* and *P. aeruginosa* were monomer and not hexamer, make them less ideal for the in vitro study (22,31).

Hexamerization is crucial for PilB in supporting its function. Assisted PilB hexamer from *M. xanthus* was observed to be ~12-fold more active than its monomer counterpart (32). Also, the activity of assisted PilB hexamer was shown to be stimulated by PilC. Something that did not happen to the monomeric PilB. The importance of hexamerization is also displayed in the GspE, a PilB homolog in the T2SS. Assisted GspE hexamer showed a solid 20-fold increase in its ATPase activity when compared to its monomeric version (33). Although exhibiting higher activity, assisted PilB hexamer might not be a good model to study PilB catalytic mechanism because the assisting protein may limit PilB domain movement. The PilB from hyperthermophilic *T. thermophilus* (*Tt*PilB) was naturally purified as a hexamer and displayed a higher ATPase activity at ~50 – 80 nmol Pi/mg PilB/minute (24,34). However, *Tt*PilB is not an ideal model for the study because it is an atypical PilB and its requirement for high temperature (34).

Despite the lack of biochemical studies in PilB, its mechanism of ATP hydrolysis can be predicted from the available structure. The structure of ATPase core *Tt*PilB and *Gm*PilB suggest that PilB hydrolyze ATP using a symmetrical rotary mechanism, consistent with the rotation model of T4P assembly (17,29,30). The structures display an elongated hexameric ring with two-fold symmetry representing a dimer of trimer. In agreement with the characteristic of symmetric rotary mechanism model, two protomers facing each other are in the same conformational state and the nucleotide turnover will direct the next event of catalysis (Figure 1-3). Thus, the activity of ATP hydrolysis is very likely to be coordinated among the pair protomer (30).
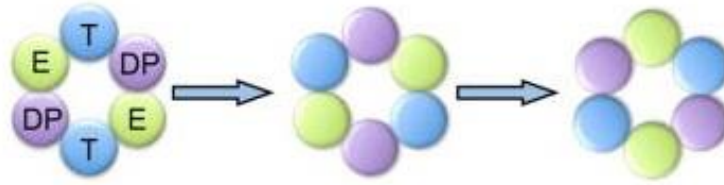
Figure 1-3. A model of symmetric rotary mechanism where a hexamer has three different conformational states; ATP bound (T, blue), ADP bound (DP, purple), and apo (E, green). The two protomers facing each other are in the same conformational state and the nucleotide turnover directs the next catalysis (35). Used under fair use, 2018.

Different conformation protomers might be reflected in its binding ability. If PilB does exhibit three different conformations of protomer, then it might have multiple affinities observed for nucleotide binding. The event of nucleotide binding by an oligomeric protein with different affinity has been observed previously in PAN ATPase. PAN, a hexameric ring proteasome the member of AAA+ ATPase, display a biphasic curve during ATP binding. The curve indicates two different affinities for ATP binding by two pairs of protomer while the last pair does not bind ATP (36).

<div align="center">**Chapter 2**</div>

<div align="center">**The type IV pilus assembly motor PilB from *Chloracidobacterium thermophilum* is a robust hexameric ATPase with complex kinetics**</div>

<div align="center">Andreas Sukmana and Zhaomin Yang</div>

This chapter is the submitted manuscript in Biochemical Journal with Dr. Zhaomin Yang as the co-author.

ZY and AS designed the experiments, AS performed the experiments, ZY and AS wrote this chapter.

ABSTRACT

The bacterial type IV pilus (T4P) is a versatile nanomachine that functions in pathogenesis, biofilm formation, motility, and horizontal gene transfer. T4P assembly is powered by the motor ATPase PilB which is proposed to hydrolyze ATP by a symmetrical rotary mechanism. This mechanism, which is deduced from the structure of PilB, is untested. Here, we report the first kinetic studies of the PilB ATPase, supporting coordination among the protomers of this hexameric enzyme. Analysis of the genome sequence of *Chloracidobacterium thermophilum* identified a *pilB* gene whose protein we then heterologously expressed. This PilB formed a hexamer in solution and exhibited highly robust ATPase activity. It displays complex steady-state kinetics with an incline followed by a decline over an ATP concentration range of physiological relevance. The incline is multiphasic and the decline signifies substrate inhibition. These observations suggest that variations in intracellular ATP concentrations may regulate T4P assembly and T4P-mediated functions *in vivo* in accordance with the physiological state of bacteria with unanticipated complexity. We also identified a mutant *pilB* gene in the genomic DNA of *C. thermophilum* from an enrichment culture. The mutant PilB variant, which is significantly less active, exhibited similar inhibition of its ATPase activity by high concentrations of ATP. Our findings here with the PilB ATPase from *C. thermophilum* provide the first line of biochemical evidence for the coordination among PilB protomers consistent with the symmetrical rotary model of catalysis based on structural studies.

INTRODUCTION

The bacterial type IV pilus (T4P) is a filamentous cell surface structure with versatile functions in many biological processes. The T4P machinery (T4PM), which is encoded by a set of *pil* genes widely distributed in bacteria, enables the construction and proper functioning of T4P in a multitude of organisms (1,37-39). Morphologically, the T4P filament is about 5-8 nm in diameter and extends a few microns beyond the cell body (7). This thin filament is assembled from membrane-embedded monomeric pilins by the T4PM which traverses the entire cell envelope of gram-negative bacteria (17,40,41). Functionally, T4P is best known for its involvement in bacterial surface motility, biofilm formation, pathogenesis and natural transformation (1,37-39). Essentially all the components of the T4PM are required for these functions, except that natural competence may only require a subset of the T4P proteins depending on the specific organisms. In bacterial pathogenesis and biofilm development, T4P mostly functions as an adhesin whereas it is the retraction of T4P that powers cell movement in bacterial motility. In addition, the T4P has been found to function in electron transport and bacterial conjugation. With the versatility of a Swiss Army knife (39), the T4PM have been investigated and dissected extensively as an extraordinary biological nanomachine.

The T4P is classified into subtype a (T4aP) and subtype b (T4bP) with structural and functional implications (1,37,38). Historically, the length of the signal sequence as well as the size and structure of the major pilin were used to differentiate T4aP and T4bP. The major prepilins of T4aP systems usually have short signal sequences and their mature pilins are also smaller than those of T4bP. As more genomes are sequenced, it has become apparent that these two subtypes can be distinguished by gene arrangements as well as the presence of selected T4P components. For example, a *pilMNOPQ* gene cluster, which has only been associated with the T4aP but not the

T4bP system, provides a reliable identifying feature of a T4aP system. While both subtypes of T4P may function in attachment, biofilm formation and competence, only T4aP has been demonstrated to mediate bacterial surface motility. It has been established that the recurrent cycle of T4aP extension and retraction is the underlying mechanism for T4P-mediated motility (9,10). That is, the distal end of an extended T4aP can be tethered or attached to a solid surface and the ensuring retraction of the T4P results in the forward motion of a bacterium. The force generated by T4P retraction can be up to 150 pN, making T4P the strongest biological motor currently known (12,13). PilT (42), which is the T4aP retraction ATPase, is present in all T4aP but only some of the T4bP systems (1). The type II secretion system (T2SS), which is related to the T4PM phylogenetically, lacks both the *pilMNOP* gene cluster and PilT (1,43,44).

The motor ATPase PilB along with other T4P proteins are responsible for the assembly and disassembly or extension and retraction of the T4aP (1,37,38). The proteins from the *pilMNOPQ* genes together with the transmembrane protein PilC appear to form a stable T4P basal body (17,21,22,45,46). Depending on its association with the PilT or the PilB ATPase, this stable basal structure allows either the retraction or extension of the T4aP filament. Presumably, if the retraction motor PilT is docked with the basal body, the pilus is retracted one pilin at a time as the T4P is dissembled at its base (17,30,42). The T4P assembly motor ATPase PilB is proposed to facilitates the reverse process or T4P extension. That is, when it associates with the basal body, it assembles the monomeric pilins embedded in the cell membrane into a growing T4P filament in a stepwise fashion. Structural studies of PilB and cryo-EM observations of the T4aP machinery *in situ* support a rotation model of T4P assembly (17,29,30,47). The N-terminal side of a PilB hexamer is proposed to directly interface with a PilC dimer on the cytoplasmic side of the cell where PilM is proposed to form a membrane-associated dodecameric ring encamping the

hexameric PilB (17). During T4P assembly, PilB would catalyze ATP hydrolysis through a rotary mechanism to rotate the PilC dimer situated in the cytoplasmic membrane (17,29,30,47). The rotating PilC would in turn scoop up the monomeric pilins from the membrane and assemble them into the growing end of the pilus (17). PilT is proposed to replace PilB and rotate PilC in the opposite direction during disassembly (17,22,45). The structure of the ATPase core of the *Thermus thermophilus* PilF/B (*Tt*PilB) and *Geobacter metallireducens* PilB (*Gm*PilB) led to a symmetrical rotary model for their catalysis (29,30,47), consistent with the rotation model of T4aP assembly supported by cryo-EM studies (17). In addition, PilB has recently been implicated in signaling in biofilm formation and c-di-GMP regulation (48,49). However, there has been no biochemical studies to support the rotary mechanisms of catalysis by PilB. The limiting factor appears to be the low ATPase activity of PilB from *Myxococcus xanthus* and *Pseudomonas aeruginosa*, the two model systems for the studies of T4P-mediate bacterial motility (22,50,51).

The report here provides the first analysis of the steady-state kinetics of PilB from the thermophilic and phototrophic bacterium *Chloracidobacterium thermophilum* (52-54). Analysis of the genome sequence of this bacterium identified a full complement of genes encoding a complete T4aP machinery. *C. thermophilum* PilB (*Ct*PilB*)* was expressed heterologously in *Escherichia coli* and purified by FPLC. Analysis indicated that *Ct*PilB is a hexamer with highly robust ATPase activity at moderate temperatures in comparison with the hyperthermophilic *Tt*PilB (55). Further studies show that this PilB displays a complex kinetic profile, consistent with it being a hexamer whose protomers hydrolyze ATP with coordination. During the course of this study, it was also discovered that there is a mutant *pilB* allele in the genomic DNA of *C. thermophilus* from an enrichment culture (53,54). The mutant PilB variant has significantly reduced ATPase activity in comparison with the wild-type. Nevertheless, both the mutant and the wild-type proteins showed

similar bi-directional kinetic profiles overall, consistent with a symmetrical rotary mechanism of ATP hydrolysis by the hexameric PilB.

EXPERIMENTAL PROCEDURES

Growth media, enzymes and chemicals―Lysogeny broth (LB) (56) was used for the growth of *E. coli* cells at 37℃. Ampicillin was supplemented at 100 µg/ml when necessary. Pyruvate kinase and L-lactic dehydrogenase from rabbit muscle were purchased from Sigma. Restriction endonucleases and other DNA modifying enzymes were from New England BioLabs. ATP and NADH were from Research Product International, Phosphoenolpyruvic acid (PEP) from Alfa Aesar Chemicals and Malachite green oxalate salt from MP Biomedicals. Media components, other common chemicals and salt were either from Fisher Scientific or Sigma.

Construction of Ct*PilB Expression Plasmids*―The coding region for *Ct*PilB was amplified by PCR using the *C. thermophilum* genomic DNA (53,54) as the template and the primers *Ct*PilB_F (CGGATCCTCAGCAAAACTTGGTGAAGT) and *Ct*PilB_R (TGACAAGCTTA GTGATGGTGATGGTGATGCAGAACCGTCTCCCGCACCA). The PCR fragment was digested with HindIII and cloned into pQE16 (Qiagen) digesting with BamHI, treated with Mung Bean Nuclease and followed by digestion with HindIII. The resulting plasmids, pAS101 and pYY101, express the wild-type *Ct*PilB and the R436C variant, respectively, with a 6×His affinity tag at their C-termini. Both plasmids were sequenced at the Genomics Research Laboratory in the Biocomplexity Institute of Virginia Tech.

Ct*PilB expression and purification*― A culture of *E. coli* with either pAS101 or pYY101 in 200 ml of LB was grown overnight at 37℃ on a rotatory shaker at 250 rpm. Six flasks containing 1 liter of LB each was inoculated with 25 ml of the overnight culture. Once the OD_{600} of these

cultures reached ~0.6 after incubation at 37°C, IPTG was added to a final concentration of 0.1 mM to initiate induction of protein expression. After 5 hours of induction at 37°C, cells were harvested by centrifugation at 4°C. The cell pellets were weighted and re-suspended at 0.2 grams per ml in cold Buffer A (25 mM Tris-HCl at pH 7.4, 500 mM NaCl, 25 mM imidazole, and 10% glycerol) with the addition of 0.3 mM PMSF and 5 mM β-mercaptoethanol. Cells were lysed by sonication using a Sonic Dismembrator (Model 300, Fisher) with 55% power for 10 cycles with 30 seconds "on" and 30 seconds "off". Cell lysis was confirmed by phase contrast microscopy. The cell lysates were centrifuged at 184,000×g for 30 min at 4°C and the supernatants were collected for the purification of *Ct*PilB.

E. coli proteins were partially removed by subjecting the supernatants to 50°C for 20 minutes followed by incubation on ice for 30 minutes. Samples were subsequently centrifuged at 184,000×g for 20 minutes at 4°C. The recovered supernatant was filtered and loaded on a 30 mL Ni-NTA column equilibrated with buffer A. Weakly bound proteins were removed by washing with buffer A. *Ct*PilB with the 6×His tagged was eluted with a linear gradient of imidazole up to 500 mM. Peak fractions were pooled, concentrated and filtered before loading on a HiPrep 26/60 Sephacryl TMS-300 column (GE Healthcare) for size exclusion chromatography. Gel filtration buffer (25 mM Tris-HCl pH 7.4, 150 mM NaCl, 2 mM TCEP, and 10% glycerol) was used for the equilibration of the column and the elution of *Ct*PilB. Fractions with *Ct*PilB were pooled and protein concentration was determined using a Bradford assay kit (BioRad). The purification process was monitored by SDS-PAGE and Coomassie Blue staining (57).

Analysis of Ct*PilB by analytical size exclusion chromatography*—2.5 mg of *Ct*PilB in gel filtration buffer was applied to a Superdex 200 10/300 GL analytical size exclusion column with a void volume (Vo) of 8.0 ml as determined by the elution of Blue Dextran. The column was

further calibrated using protein markers with molecular weights (MWs) of 29 kDa, 69 kDa, 200 kDa, 443 kDa and 669 kDa (Sigma). The elution of *Ct*PilB was monitored by UV absorption and its apparent MW was calculated based on its elution volume (Ve) and those of the MW standards.

Optimization of conditions for the Ct*PilB as an ATPase*—An endpoint assay based on the Malachite Green (MLG) method (58) measuring the levels of phosphate was used to optimize the condition for the ATPase activity of *Ct*PilB. Each reaction was set up with 5.2 µg/ml of *Ct*PilB and 1.5 mM ATP with varying buffers and salts in a PCR tube. The reactions in PCR tubes were allowed to occur at desired temperatures in an Eppendorf Mastercycler gradient thermocycler for 15 minutes before switching to 4°C for the stoppage. Reactions with buffer instead of *Ct*PilB or ATP were included as negative controls. An aliquot of each reaction mix was transferred to a 96-well plate which included a concentration series of KH_2PO_4 as phosphate standards. MLG reagents (0.034% MLG, 10 mM Ammonium molybdate 1 N HCl, 3.4% EtOH and 0.01% Tween 20) were mixed into each well and incubated for 10 minutes at room temperature before the absorbance at 620 nm was measured using a Tecan SPECTRAFluor Plus plate reader. The amount of phosphate in each sample was calculated against the standard curve constructed from the KH_2PO_4 concentration series. The activity of *Ct*PilB was computed by dividing the amount of phosphate (in nanomole) by the amount of protein (in milligram) and the reaction time (in minutes) and expressed in nmol Pi/mg PilB/min. All assays were performed in triplicates for each experiment.

Studies of steady-state kinetics of the Ct*PilB ATPase*—The buffer used for kinetic studies of *Ct*PilB by the MLG assay contained 50 mM of TAPS (N-[Tris(hydroxymethyl)methyl]-3-aminopropanesulfonic acid) and Tris each at pH 8.7, 75 mM KCl, 50 mM NaOAc, 5 mM $MgCl_2$, and 50 µM $ZnCl_2$. For experiments with 12 different [ATP], aliquots from reactions with *Ct*PilB at 5.2 µg/ml were withdrawn after 1, 2, 3 and 4 minutes of incubation at 54°C. For those with 16

different [ATP], samples were taken at 1, 2 and 3 minutes. These samples were quickly put on ice at their respective time points and trichloroacetic acid (TCA) was added to a final concentration of 4% to inactivate PilB. The amount of phosphate in each sample was quantified using 96-well plates as described above. The amounts of phosphate were plotted against time for each ATP concentration and the rate of ATP hydrolysis was calculated from the slope of the curve. Preliminary experiments with different [ATP] established that the amounts of phosphates released from ATP hydrolysis by CtPilB remained linear up to 8 minutes within the [ATP] range used in this study under our experimental conditions. Non-enzymatic hydrolysis of ATP was below the detection limit of the MLG assay within the timeframe of these experiments under our experimental conditions, which is consistent with a previous report (59).

The kinetic of CtPilB was additionally analyzed by an enzyme-coupled ATPase assay (60,61) at 37°C using the optimum buffering condition as determined above. In this assay, the ADP generated by ATP hydrolysis is enzymatically converted back to ATP with the oxidation of NADH to NAD^{+}. The decrease in NADH can be detected by the decrease in absorbance at 340 nm. The reactions, which were optimized prior to the kinetic studies of CtPilB, contained pyruvate kinase at 20 U/ml, L-lactic dehydrogenase at 20 U/ml, 4 mM PEP, 0.5 mM NADH, and varying concentrations of ATP. The experiments were conducted at 37°C with a reaction volume of 200 µl per well in a 96-well plate with CtPilB at 52 µg/ml. The absorbance at 340 nm was monitored at one-minute intervals using a Tecan Infinite F200 Pro plate reader with temperature control. The rate of ATP hydrolysis was calculated by the slope of the absorbance over time in the linear range. Data analysis and calculations were performed using Microsoft Excel and curve fitting was conducted with KaleidaGraph Version 4.5.

Kinetic study of the Ct*PilB(R436C) variant as an ATPase*—The kinetic analysis of the Ct PilB(R436C) ATPase in steady-state was conducted using the same procedure and the MLG assay as for the wild-type *Ct*PilB except that the amount of *Ct*PilB(R436C) was 21.0 µg/ml.

Structural modeling of Ct*PilB*—The structural model of *Ct*PilB was generated by the SWISS-MODEL (62) using the hexamer of the *Tt*PilB ATPase core (29) as the template. The visualization and representation of the structure were performed using the PyMOL (63).

RESULTS

Chloracidobacterium thermophilum *has a full complement of genes for T4aP* — The photosynthetic thermophilic acidobacterium *C. thermophilum* was first discovered in a microbial mat of hot spring in the Yellow Stone National Park, WY (52-54). Our analysis of its genome sequence (54) indicated that it has a full complement of *pil* genes for the machinery of a T4aP system (Figure 2-1A). All the *pil* genes are encoded on the first of its two chromosomes and the most conserved among them are clustered at two genetic loci. One cluster, which includes *pilM, pilN, pilO, pilP,* and *pilQ,* likely forms an operon with all ORFs reading on the negative/Crick strand of the chromosome. The other locus has *pilB, pilT,* and *pilC* genes, all three reading on the positive/Watson strand. The presence and the arrangement of the *pilMNOPQ* gene cluster indicates that *C. thermophilum* likely assembles a T4aP (1,37,38), which is consistent with the presence of *pilT* in the *pilBTC* cluster. Aside from another gene cluster for a probable T2SS, there are four other genes on this chromosome elsewhere encoding proteins with a prepilin-type signal sequence. Analysis suggests that CABTHER_RS02295 may encode the major pilin for the T4aP pilus of *C. thermophilum* while the other three minor pilins.

The arrangements of these *pil* genes in *C. thermophilum* resemble those in the δ-proteobacteria including *M. xanthus* (38), a model organism for studies of T4aP-mediated motility and functions (23,64,65). This is in agreement with the close relationship of Chloracidobacteria with the δ-proteobacteria on the phylogenetic tree (66). Further sequence analysis indicates that the *C. thermophilum* PilB (*Ct*PilB) is a T4aP assembly ATPase ortholog that aligns well with *M. xanthus* PilB (*Mx*PilB) (Figure 2-1B) and PilB in other T4aP systems (Figure S1). Among the best studied PilB orthologs, *Ct*PilB shows the highest amino acid identity with PilB from *M. xanthus* and *G. metallireducens*, both of which are δ-proteobacteria that share a common root with

acidobacteria on the phylogenetic tree (66). In addition, a chimera containing the N-terminus of *Mx*PilB and the C-terminus of *Ct*PilB supported T4P-mediated motility in *M. xanthus* (Figure S2), indicating that *Ct*PilB is likely functional *in vivo* and a reasonable candidate for the studies of the PilB ATPase *in vitro*.

Purification of Ct*PilB* — *Ct*PilB with a 6×His tag fused to its C-terminus was expressed and purified using *E. coli* as a host (Figure 2-2). Briefly, the coding region of *pilB* was PCR amplified from *C. thermophilum* genomic DNA (kindly provided by Dr. Donald Bryant at The Pennsylvania State University) (54) and cloned into an IPTG-inducible expression vector. *E. coli* cells containing the recombinant expression plasmid were induced with IPTG to produce *Ct*PilB. The soluble fraction of the whole cell lysates after a mild heat treatment was subjected to Ni-NTA affinity chromatography where *Ct*PilB eluted around 180 mM imidazole. *Ct*PilB was further purified by preparative size exclusion chromatography (SEC) where it eluted as a single peak, indicating uniformity of the oligomeric state of the purified protein.

Ct*PilB is a hexamer* — The oligomeric state of the purified *Ct*PilB was examined by analytical SEC with a column calibrated with protein standards of known molecular weight (MW) (Figure 2-3A). On this column, *Ct*PilB eluted as a single peak centered at the elution volume of 10.25 ml (Figure 2-3A). This corresponds to an apparent MW of 422 kDa based on the standard curve from the elution of the MW markers (Figure 2-3B). This apparent MW is 6.12 times of 68.9 kDa, the theoretical MW of a *Ct*PilB monomer with the 6×His tag. In addition, *Ct*PilB was analyzed by dynamic light scattering (DLS) in gel filtration buffer (Supplementary Figure S3A), which indicated a hydrodynamic diameter of 240 Å. This size is about 100 Å larger than the diameter of the crystal form of the hexameric ATPase core of *Tt*PilB which lacks the conserved N-terminus (Figure 2-1B) (29). It is also more than 50 Å larger than the PilM ring where PilB is

proposed to fit (17). It appears therefore that *Ct*PilB exists *in vitro* in a more extended form in solution than expected, which may explain the slight increase in its apparent molecular weight by SEC (Figure 2-3) over a theoretical hexamer of *Ct*PilB. These results here indicate that the purified *Ct*PilB is a hexamer, which is in contrast with *M. xanthus* PilB that purified as a monomer without a hexameric tag (22,50).

Ct*PilB is a thermophilic ATPase requiring Mg^{2+} and Zn^{2+} for its activity* ― The ATPase activity of *Ct*PilB was analyzed and optimized initially by an endpoint assay using the Malachite Green (MLG) method which measures the amount of phosphate released from ATP hydrolysis (67,68). The optimum buffering conditions were found to require 50 mM of TAPS and Tris each, 75 mM KCl and 50 mM NaOAc at the optimum pH of 8.7 (Figure 2-4A). As was expected for a member of the PilB ATPase family (24,29), *Ct*PilB requires Mg^{2+} as well as Zn^{2+} for activity with the optimum concentration at 5 mM and 50 µM, respectively (Figure 2-4B). The optimum temperature for the ATPase activity of *Ct*PilB was determined to be ~54°C (Figure 2-4A), consistent with the temperature of the hot spring where *C. thermophilus* was first discovered (52-54).
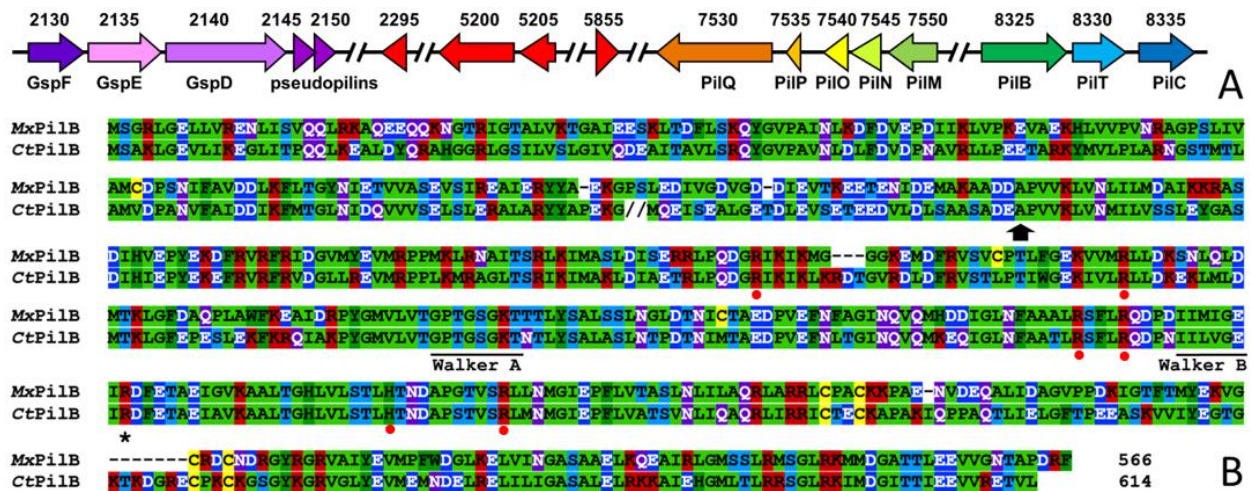
Figure 2-1. T4P and T2SS components encoded on the *C. thermophilum* genome. (A) Open reading frames (ORFs) for *C. thermophilum* T4P and T2SS proteins. The sizes and directions of all ORFs are drawn to scale and according to their relative positions on the first chromosome of *C. thermophilus* with double slashes (//) indicating breaks in the continuity of the sequences. Indicated above each ORF is its CABTHER_RS locus tag and below is its homology to either a T2SS protein by the Gsp designation or a T4P or Pil protein by the nomenclature in *M. xanthus* and *P. aeruginosa*. ORFs with prepilin-like signal sequences are colored red. For scale, the GspF ORF is 405 amino acids long. (B) Alignment of *Ct*PilB with *Mx*PilB. Residues are colored by charge, polarity and hydrophobicity. Walker A and Walker B residues in *Ct*PilB are underlined. The asterisk (*) marks Arg-436 that is changed to a Cys in the published genome of *C. thermophilum.* The red dots (•) mark the additional conserved residues lining the surface of a channel with the proposed function of escorting the phosphate from ATP hydrolysis to exit the active site of PilB (29). The arrow indicates the start of the *Ct*PilB ATPase corresponding to and modeled after the crystal structure of *Tt*PilB.
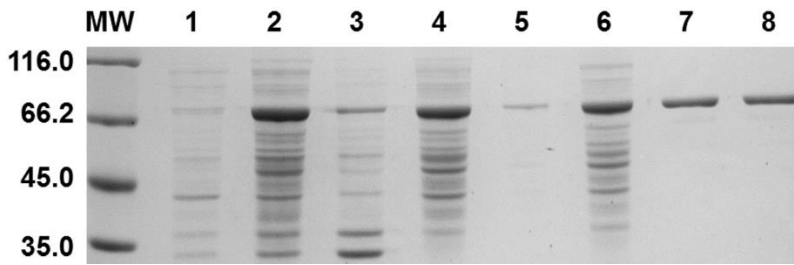
Figure 2-2. Purification of *Ct*PilB. Samples were run by SDS-PAGE and stained by Coomassie Blue. The leftmost lane was loaded with Molecular Weight (WM) standards with mass in kilodalton (kDa) indicated to the left. Lane 1, whole cell lysate before induction; Lane 2, whole cell lysate after induction; Lanes 3 and 4, insoluble and soluble fractions from Lane 2; Lanes 5 and 6, insoluble and soluble fractions after a mild heat treatment; Lanes 7 and 8, pooled *Ct*PilB fractions after Ni-NTA affinity and size exclusion chromatography.
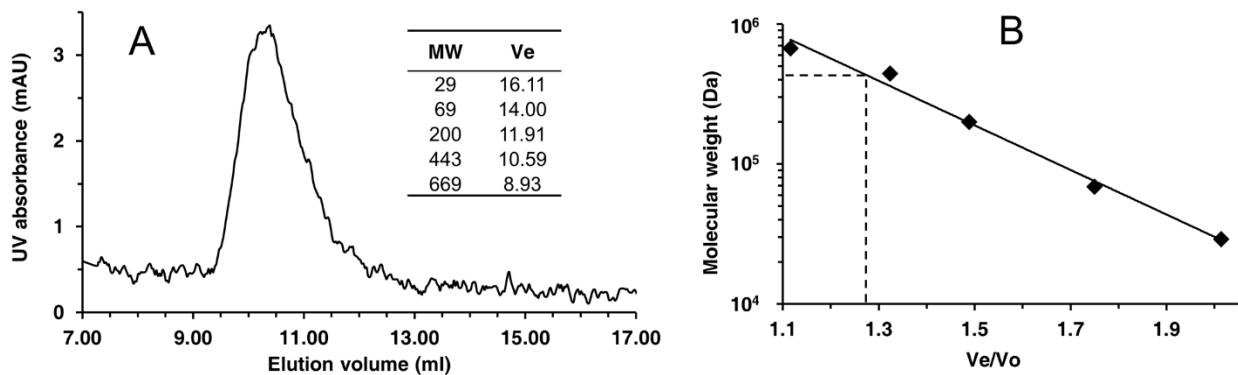
Figure 2-3. Molecular weight of *Ct*PilB determined by analytical size exclusion chromatography. (A) Chromatogram showing the elution volume (Ve) of ~10.25 ml for *Ct*PilB from analytical SEC. The SEC column was calibrated with five protein standards, and their MW in kDa and Ve in ml are provided in the table in the panel. The void volume (Vo) of the column is 8.00 ml as determined by the elution of blue dextran. (B) A standard curve was generated by plotting the MW of the standards against their Ve/Vo. The elution volume for *Ct*PilB correlates to an apparent MW of 422 kDa on this curve as indicated by the dashed lines.

CtPilB is a highly robust ATPase ─ Steady-state kinetics of *Ct*PilB was first analyzed at 54°C using the MLG assay and the conditions as optimized above. The rates of ATP hydrolysis remained linear up to 8 minutes in our assay for all ATP concentrations and the initial rate was calculated using time points up to 4 minutes (Figure 2-5A). As shown in Figure 2-5B, the activity of *Ct*PilB shows a bidirectional response to increasing concentrations of ATP. The rate of ATP hydrolysis steadily rose with increasing [ATP] initially, approaching the highest at ~1.5 mM ATP (Figure 2-5B). Interestingly, a slower rate of ATP hydrolysis is observed when [ATP] increased further. The kinetic profile of *Ct*PilB can therefore be divided into two parts, an incline followed by a decline with a peak around 1.5 mM ATP. The highest activity previously reported for a PilB ATPase was ~20 nmol/mg/min for the hexameric *Tt*PilB (55). The activities reported for PilB from mesophiles *M. xanthus* and *P. aeruginosa* were between 3 to 10 nmol/mg/min (22,50,51,69). In comparison, the purified *Ct*PilB is a more robust ATPase that can hydrolyze ATP over 700 nmol/mg/min (Figure 2-4).

CtPilB ATPase exhibits substrate inhibition ─ The results in Figure 2-5B indicated that the rate of ATP hydrolysis by *Ct*PilB increased with increasing [ATP] until about 1.5 mM. The incline turns to a decline with further increase in [ATP]. We next analyzed *Ct*PilB in an [ATP] range ≥1.2 mM with increasing data density to focus on the decline of *Ct*PilB kinetics (Figure 2-6A). The results confirmed the bidirectional nature of the response of *Ct*PilB to [ATP]. The highest rate of ATP hydrolysis by *Ct*PilB, about 700 nmol/mg/min, was observed at 1.5 mM. Either higher or lower [ATP] resulted in lower rate of ATP hydrolysis. The declining slope at higher [ATP] suggests that *Ct*PilB as an ATPase is inhibited by its substrate ATP.
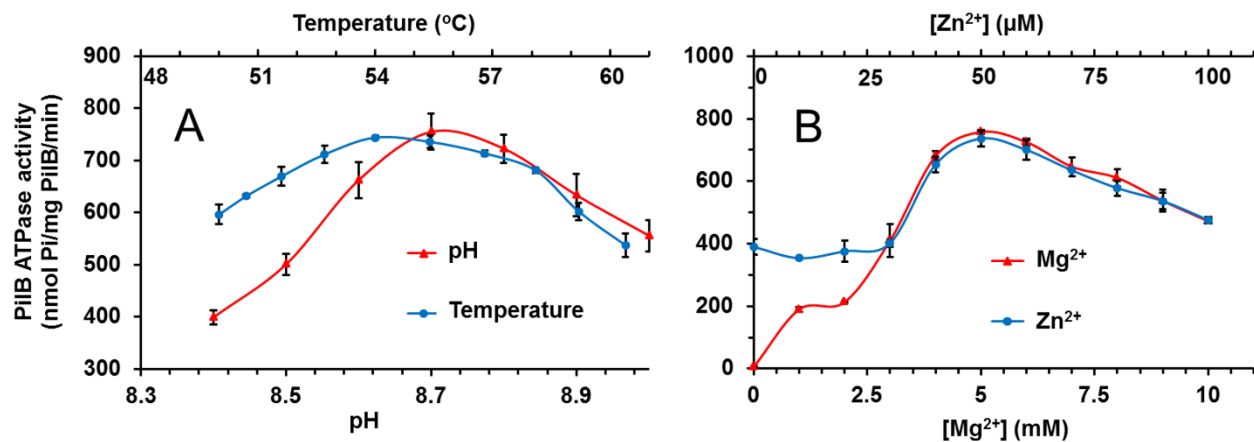
Figure 2-4. Optimization of assay conditions for the *Ct*PilB ATPase. An endpoint MLG assay was used for the experiment. Shown is the dependency of *Ct*PilB ATPase activity on pH and temperature (A) or concentrations of Mg^{2+} and Zn^{2+} (B). Unless noted otherwise, all reactions were performed at 54°C with 5.2 μg/ml of *Ct*PilB in a buffer containing 50 mM of TAPS and Tris each at pH 8.7, 75 mM KCl, 50 mM NaOAc, 5 mM Mg^{2+}, 50 μM Zn^{2+} and 1.5 mM ATP. Error bars represent standard deviations from three independent experiments each performed in triplicates.
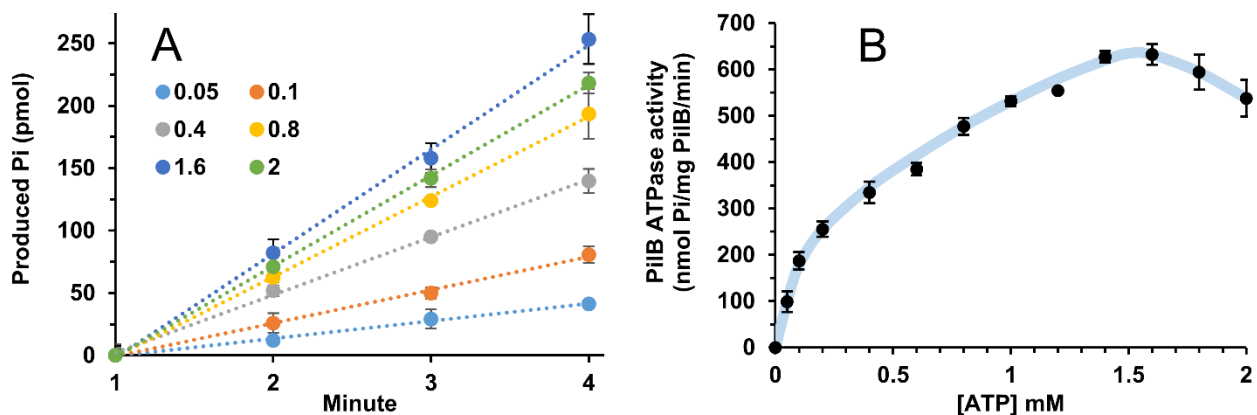
Figure 2-5. Steady-state kinetics of *Ct*PilB ATPase. Kinetics of the *Ct*PilB ATPase was analyzed at 54°C using the MLG assay. (A) The amounts of phosphate in each reaction with the indicated ATP concentration are normalized to 0 for the 1 minute time point and plotted over time. The experiments were performed in triplicates for every time point at each ATP concentration with the error bar representing the standard deviation from the triplicate samples. For clarity, only the data for selected ATP concentrations are shown. The initial rate of ATP hydrolysis was calculated from the slope at each ATP concentration. (B) The rates of ATP hydrolysis by *Ct*PilB are plotted against their corresponding ATP concentrations. Results are from three independent experiments with means and standard deviations indicated. An arbitrary trend line is drawn through the data points as a guide.

23

However, during the time course of the ATPase assay, ATP is hydrolyzed to ADP which accumulates over time. It was theoretically possible that the accumulation of ADP inhibited the ATPase activity (70-72) of CtPilB at high [ATP] even before the first sample could be taken at 1 minute (Figures 2-5A and 2-5B). In addition, because the ATP stock used in the experiment contained trace amounts of ADP (Alfa Aesar), the increase in [ATP] led to a concurrent increase in ADP concentrations in the reactions even before enzymatic hydrolysis of ATP occurred. To examine if CtPilB displays ATP or substrate inhibition, an enzyme-coupled ATPase assay (60) was used additionally to study the kinetics of CtPilB . In this assay, ADP produced from ATP hydrolysis is continuously converted back to ATP by two other enzymes with the oxidation or expenditure of NADH stoichiometrically. The decrease in NADH can be continually monitored by spectrophotometry for kinetic studies. As a consequence, ATP is maintained at a constant concentration and there would be no significant accumulation of ADP over the course of the assay. Because two other enzymes are present in this assay, it was performed at 37°C. The highest rate for the CtPilB ATPase (Figure 2-6B), obtained from the linear range of this assay (Figure 2-6B, insert), is significantly reduced in comparison with the activity at 54°C (Figure 2-6). Analysis using the MLG-based assay at 37°C confirmed the temperature-dependent reduction of CtPilB activity at 37°C (Figure S4). Despite the differences in the overall kinetic profile at these two temperatures, the rate of ATP hydrolysis by CtPilB clearly decreased at the higher range of [ATP] at 37°C (Figures 2-6B & S4). That is, the ATPase activity of CtPilB decreased with increasing [ATP] beyond 1.5 mM. The result (Figure 2-6) here indicate that the CtPilB ATPase is inhibited by its substrate ATP at high concentrations.
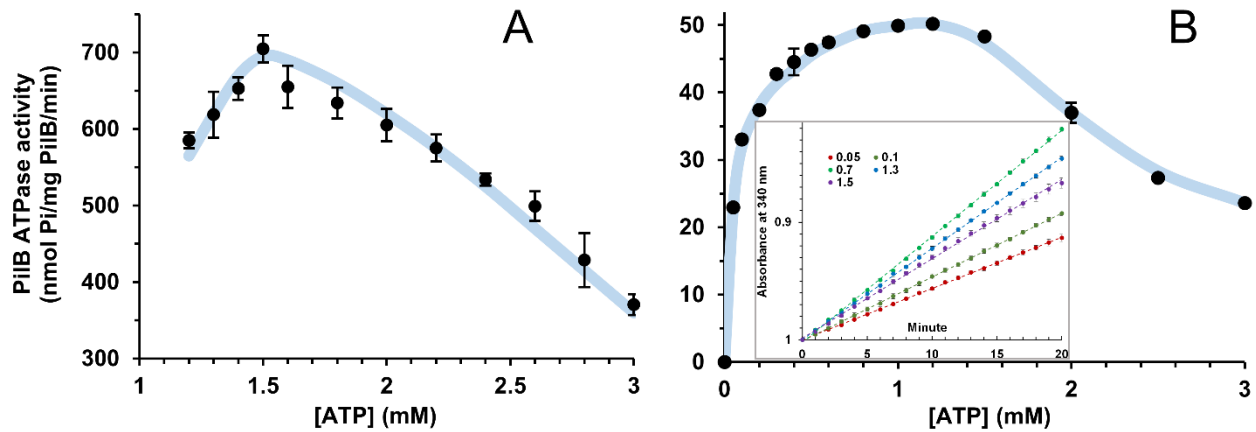
Figure 2-6. Substrate inhibition of *Ct*PilB ATPase. (A) MLG assays were performed as in Figure 2-5B. (B) The rates of ATP hydrolysis by *Ct*PilB were determined at 37°C using the enzyme-coupled assay. Results from three independent experiments are presented in each panel as in Figure 2-5B with an arbitrary trend line. The insert in panel B illustrates linearity of the assay over time after preincubation in the chamber of the plate reader set at 37°C (note that the Y axis in the reverse order). To avoid clutter, only the results for five ATP concentrations from one experiment are shown in the insert.
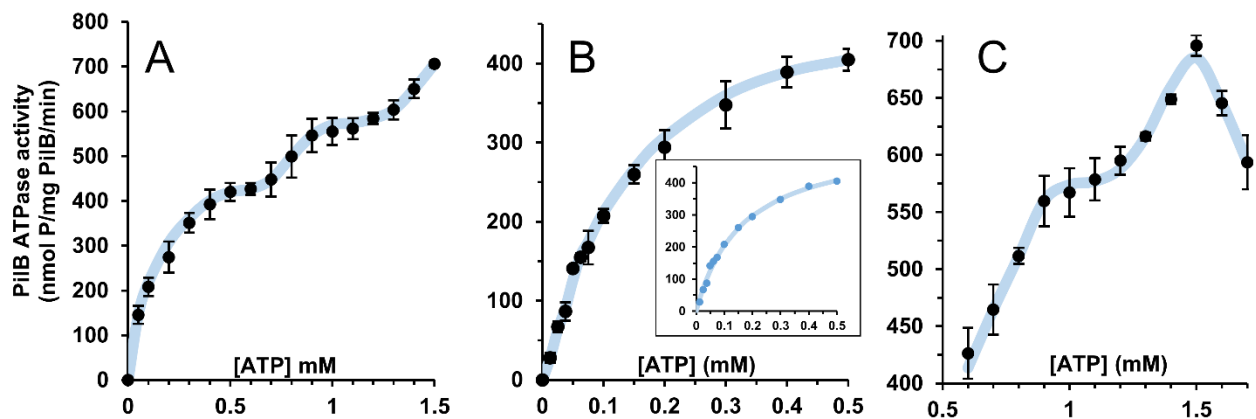
Figure 2-7. The incline of *Ct*PilB ATPase kinetics is multiphasic. The kinetic profile of *Ct*PilB ATPase in the [ATP] range from 0 to 1.5 mM (A), 0 to 0.5 mM (B) and 0.6 to 1.7 mM (C). The insert in panel B indicates the fit of the average to Michaelis-Menten equation. Experiments and data presentation are the same as in Figure 2-5B.

25

The incline in the kinetics of Ct*PilB ATPase is multiphasic* —The rates of ATP hydrolysis by *Ct*PilB at ≤1.5 mM ATP showed an upward trend with increasing [ATP]. However, no significant plateau or saturation in activity was observed at the high end of [ATP] as would be expected if *Ct*PilB had conformed to Michaelis-Menten kinetics (Figure 2-5B). We subsequently analyzed *Ct*PilB ATPase activity with increased data density in the concentration range of 0 to 1.5 mM ATP (Figure 2-7A) to further our understanding of *Ct*PilB kinetics. The data here show clearly that *Ct*PilB kinetics presents a triphasic profile with three regions of steady increase in activity with increasing [ATP]. *Ct*PilB ATPase activity rose at low [ATP] and reached a first plateau around 0.5 mM ATP. A second upward shift followed with an ensuing plateau around 1.1 mM ATP before a third upward shift is observed. *Ct*PilB, as a hexameric ATPase, is thus not an enzyme with simple Michaelis-Menten kinetics. Instead, it employs a more complex mechanism to carry out its cycle of ATP hydrolysis.

Nevertheless, a preliminary analysis suggested that the rate of ATP hydrolysis by *Ct*PilB at [ATP]≤0.5 mM (Figures 2-5B & 2-7A) might follow the Michaelis-Menten steady-state kinetics. We therefore analyzed the rate of ATP hydrolysis by *Ct*PilB in this concentration range with increased data density (Figure 2-7B). Analysis indicates that the data in this [ATP] range obey Michaelis-Menten kinetics (Insert in Figure 2-7B). Curve fitting produced a theoretical V_{max} of 541 nmol/mg/min and a K_m of 0.164 mM with an R^2 value of 0.996. These results indicate that *Ct*PilB follows the steady-state kinetics of a simple enzyme at sub-millimolar concentrations of ATP despite its more complex kinetics at higher [ATP].

We next focused on the kinetics of *Ct*PilB in the [ATP] range around 1.0 mM with increasing data density (Figure 2-7C). This new data set recapitulated the bidirectional nature of the kinetic profile of *Ct*PilB (Figures 2-5B & 2-6), showing peak activity at 1.5 mM ATP and

lower hydrolysis rate on both sides of the curve (Figure 2-7C). More importantly, these results confirmed the second upward shift and the plateau around 1.0 mM ATP in *Ct*PilB activity (Figures 2-7A and 2-7C). We have been unable to achieve any reasonable fit for the data in Figures 2-7A & 2-7C to established enzyme kinetic equations, indicating complicated effects of ATP on the ATPase activity of *Ct*PilB.

A conserved arginine is important for Ct*PilB activity*—During the cloning and sequencing of the constructs for *Ct*PilB expression in this study, it became apparent that there were two versions or alleles of *pilB* present in the *C. thermophilum* genomic DNA, which was isolated from cells that were fractionated from a mixed culture by differential centrifugation (53,54). One version, which encodes the amino acid sequence presented in Figure 2-1B, is designated as the wild type in this study. Its protein was used for all the results presented thus far (Figures 2-7). The other version, which is in the published genome sequence of this organism (54), has a single nucleotide polymorphism changing a CGT codon to TGT. This results in the substitution of Arg-436 with a Cys (R436C) in *Ct*PilB. This Arg, which resides adjacent and C-terminal to the Walker B box (Figure 2-1B), is strictly conserved in PilB and related ATPases (22). Structural modeling based on the crystal structure of *Tt*PilB (29) indicated that this Arg residue contributes to the positively charged surface of a channel between two adjacent protomers leading to a bound ATP molecule (29) (Figure 2-8A). It is noted that Arg-436 is distinct from the Arg finger residues (Arg-293 and Arg-310) of *Ct*PilB residing N-terminal to the Walker A box (Figure 2-1B) (29).

To examine the effect of the R436C substitution on *Ct*PilB activity, the *Ct*PilB(R436C) variant was expressed and purified similarly as the wild-type *Ct*PilB for studies *in vitro*. DLS analysis of *Ct*PilB(R436C) indicated a similar particle size (data not shown) as the wild-type *Ct*PilB (Figure S3). As shown in Figure 2-8B, the maximum activity of the *Ct*PilB(R436C) variant

as an ATPase was reduced to <40 nmol/mg/min at 54°C, a 18× fold change in comparison with its wild-type counterpart under the same assay conditions. This result indicates that a R436C mutation likely impacts T4P assembly significantly at the cellular level *in vivo*. Nevertheless, the overall kinetic profile of this *Ct*PilB mutant variant largely resembled that of the wild type (Figure 2-5B). That is, its ATPase activity increased with increasing [ATP] up to 1.5 mM and higher [ATP] inhibited its activity as was observed with the wild type (Figure 2-5A). These results, while confirming that *Ct*PilB ATPase is inhibited by its substrate ATP at high concentrations, indicate that the highly conserved Arg-436 neighboring the Walker B box is crucial for the ATPase activity of PilB.
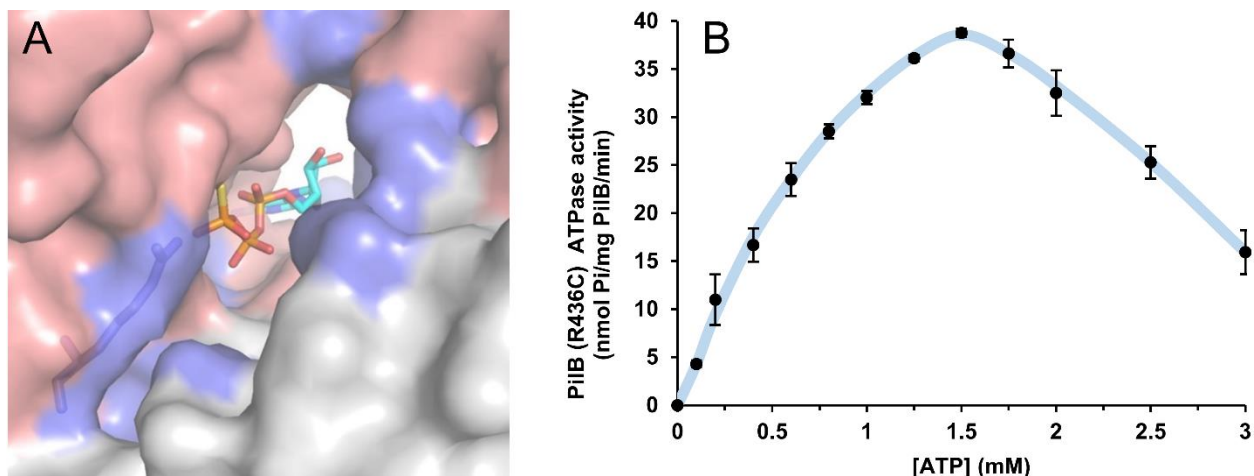
Figure 2-8. ATPase activity of *Ct*PilB(R436C) is severely reduced. (A) The close-up view of a channel in the structural model of the wild-type *Ct*PilB generated based on *Tt*PilB (29,62). This channel, which is formed by two neighboring protomers colored in either light maroon or gray, is proposed to escort the exit of the phosphate from ATP hydrolysis. The blue patches indicate the surfaces contributed by the positively charged Arg-436 (in sticks) as well as Lys, His and other Arg residues (also see Figure 2-1B). At the back of the channel is an ATP-γ-S in the ATP binding pocket modeled in from the crystal structure of *Tt*PilB. (B) Steady-state kinetics of *Ct*PilB(R436C). Kinetic study of *Ct*PilB(R436C) was conducted using the same conditions as in Figure 2-5A except that 21 µg/ml of *Ct*PilB(R436C) was used in the assay.

DISCUSSION

We demonstrate here that *Ct*PilB is a natural hexamer (Figures 2-2 and S3) with robust ATPase activity *in vitro* (Figures 2-5, 2-6, 2-7 & S5). At the cellular level, the activity of PilB is expected to correlate with the rate of T4P assembly observed *in vivo*. *P. aeruginosa* T4aP extends about 0.5 μm per second (10). Since the change in length is 8-10 Å per pilin in the T4P filament (7), this rate of extension translates to ~500 pilins processed by one T4PM per second or 30,000 per minute. In the current model, one T4PM is associated with one PilB hexamer (17). If we consider an expenditure of 2 ATPs per assembled pilin (17,29,30,73), 60,000 ATPs would be hydrolyzed per minute per PilB hexamer during active T4P assembly. *Tt*PilB, an atypical hyperthermophilic PilB with a long N-terminal extension, hydrolyzed 13 ATPs per minute per hexamer *in vitro* (55). PilB from the mesophiles *M. xanthus* and *P. aeruginosa* hydrolyzed 1-3 ATPs *in vitro* per minute per hexamer equivalent (22,50,51). In comparison, the highest rate of ATP hydrolysis by *Ct*PilB here translates to about 290 ATPs per minute per hexamer. This improvement in activity allowed the first kinetic studies of PilB, providing biochemical insights into the catalytic mechanism of PilB for the first time. On the other hand, the activity of *Ct*PilB reported here is still more than two orders of magnitude below the T4P assembly rate *in vivo*, suggesting that other T4P proteins in or exposed to the cytoplasm play significant roles in stimulating the activity of PilB during T4P assembly. For perspectives, a bacterial cell with a volume of 1.0 cubic micrometer (74) would contain ~600,000 ATP molecules at a given moment at 1 mM intracellular [ATP]. The ATP pool is replenished in part by the bacterial F_0F_1 ATP synthase which has a turnover rate up to ~12,000 molecules per minute per enzyme *in vitro* (75). This enzyme can also function in the reverse as a rotary motor ATPase capable of hydrolyzing ~300,000 ATP molecules *in vitro* at an optimum temperature (76). The rate of *Ct*PilB as an ATPase

29

is ~1,000-fold lower in comparison despite its higher activity than its counterparts currently in the literature (22,50,51).

The steady-state kinetics of *Ct*PilB exhibits two striking features (Figures 2-5, 2-6, 2-7 & S5) that distinguish it from Michalis-Menten kinetics. One is substrate inhibition as signified by the downward shift or the decline in the kinetics of *Ct*PilB at high [ATP]. The other is the multiphasic nature of the kinetic incline before the decline starts at [ATP]>1.5 mM. The size of *Ct*PilB as determined by DLS (Supplementary Figure S3B) was unchanged in the presence and absence of a non-hydrolyzable ATP analogue in the enzyme activity buffer. The reduced ATPase activity of *Ct*PilB at high concentrations of ATP is therefore not due to the disintegration of the *Ct*PilB hexamer into monomers or lower orders of oligomers. We suggest that these complex kinetics behaviors reflect coordination among protomers and the highly dynamic nature of *Ct*PilB as a hexameric ATPase *in vitro*. These observations are consistent with the proposed rotary models of catalysis by PilB and of the T4P assembly by T4PM (17,29,30,47) as discussed next.

The substrate inhibition of *Ct*PilB may be explained by increased rigidity when ATP occupies the binding sites of all six protomers of a PilB hexameric ring. Simulations based on the crystal structure of PilB and the rotary mechanism suggest that the conformational changes of the three pairs of PilB protomers are highly coordinated (29). The proposed mechanism of force generation by PilB as a motor ATPase requires the dynamic and fluid movement of all protomer pairs in sync as hinged blocks (29). This means that the coordinated movement among the different protomers requires the overall fluidity of the hexameric ring during catalysis. As such, increased rigidity across the hexameric ring is expected to interfere with the requirement of such dynamic movements during the ATP hydrolytic cycle. It is possible that the two-fold symmetry of PilB, which is considered to be critical for its ATPase activity in the current model (29,30,47), may be

broken at high [ATP]. The *Archaeoglobus fulgidus* hexameric ATPase GspE, which crystallized as an asymmetric hexamer, was found to assume a six-fold symmetry at high concentrations of an ATP analog, for example (77). This lends support to the proposed mechanism of substrate inhibition described above. This mechanism is also reminiscent of the inhibition of the hexameric ATP synthase by ADP (78,79). In this case, the cooperativity among the protomers is blocked by excess ADP as a substrate which entraps this rotary enzyme in an inhibited state. There are additional models for substrate inhibition (80) that may apply to *Ct*PilB as well. In this context, there are at least two other hexameric ATPases, RuvB and 26S proteasomes, that are known to be similarly inhibited by ATP at high concentrations (81-83).

The rise and saturation of *Ct*PilB activity prior to substrate inhibition do not obey classical Michaelis-Menten kinetics either (Figures 2-5, 2-7 & S5). Instead, there are perhaps three phases in the incline prior to the decline at >1.5 mM ATP. The first phase covers [ATP] up to 0.5 mM, the second from 0.6 to 1.1 mM and the third from 1.2 to 1.5 mM. The first phase fits the Michaelis-Menten equation quite well (Figure 2-7C). That is, in the sub millimolar [ATP] range, *Ct*PilB behaves as a simple ATPase with a K_m around 0.16 mM and its activity plateaus around 0.5-0.6 mM ATP (Figure 2-7B). As [ATP] increases further, the activity of *Ct*PilB rises again until it reaches a second plateau around 1.0 mM ATP. In the third phase, the activity of *Ct*PilB further elevates until it peaks at 1.5 mM ATP. The increases in *Ct*PilB activity in the latter two phases can be explained by the engagement of additional active sites or protomers for catalysis in the hexamer at high [ATP] (80). That is, it is reasonable to assume that at a given moment, the protomers within an asymmetric hexamer may have different binding affinities for the substrate (29,30,36), resulting in multiple K_m values in kinetics. Alternatively, these increases could be due to allosteric regulation by ATP binding to additional protomers in the hexamer. The observations with *Ct*PilB are

31

reminiscent of the non-Michaelis-Menten kinetics of the Na^+/K^+ ATPase (84) and the relief of attenuation of the RuvB ATPase by additional ATP (81,82). Coordination and allosteric influence among promoters of these hexameric ATPases are provided as possible explanations of these observations (82,84). If a PilB hexamer has one pair of protomers hydrolyzing ATP simultaneously as proposed in the symmetrical rotary model (29,47), the interaction of nucleotides with the ATP binding pockets of a third or additional protomers may allosterically stimulate the overall activity of the hexamer (80-82). ATP binding to neighboring subunits and intersubunit allosteric coupling is recently proposed to underlie the function of proteasomal ATPases (85). It is also possible that ATP may interact with unknown binding sites on the enzyme to exert an allosteric regulation (29,48,80,82).

The different phase of the kinetics of *Ct*PilB (Figures 2-5, 2-6, 2-7 & S5), including substrate inhibition, all occur within physiologically relevant concentrations in bacteria. The intracellular [ATP] in bacteria can vary from below 1 mM to more than 3 mM (86-91). The fluctuation in cellular [ATP] may be attributed to bacterial growth phase (88) and media compositions (92). For photosynthetic cyanobacteria, intracellular concentrations of ATP may vary in response to light and circadian rhythm (89,93). Since *C. thermophilum* is a photosynthetic bacterium (52,53), its intracellular ATP concentration is likely responsive to light conditions and periodicity. In addition, it is known that the cyanobacterium *Synechocystis* regulates its T4P-mediated motility to perform phototaxis (94,95). The cellular localization of PilB tends to correlate with the direction of T4P-mediated motility in *M. xanthus* and *Synechocystis* (45,96). As such, the regulation of PilB activity by ATP may influence tactic and motility behavior *in vivo*. Heterogeneity in T4P-mediated motility has been observed in *M. xanthus* (45), *P. aeruginosa* (97) and *Synechocystis* (95). That is, only a sub population of bacterial cells are actively motile under

the same growth conditions. While the reasons for this heterogeneity is not understood, variations in intracellular [ATP] (87) and their effects on PilB activity may partially contribute to this heterogeneity at the population level. In addition, nutrient levels are known to influence *M. xanthus* motility (98), and differences in ATP levels under varying conditions may modulate T4P-mediated bacterial surface motility. It is noted that the substrate inhibition of RuvB and 26S proteasomes also occurs at physiologically relevant concentrations of ATP (81-83).

We designated the *Ct*PilB with Arg-436 as the wild type (Figures 1B & 2-8A). For one, this Arg is strictly conserved in the sequences of related ATPases (22). For another, the draft genome of another *C. thermophilum* became available recently (99) and it has an Arg instead of a Cys in the same position of *Ct*PilB. This conserved Arg is no doubt critical for the activity of *Ct*PilB as an ATPase (Figure 2-8) and the *Ct*PilB(R436C) variant likely results in phenotypic heterogeneities in piliation if it exists in nature. Based on the crystal structure of *Tt*PilB, this conserved Arg lines the surface of a positively charged channel that is proposed to escort the exit of the negatively charged phosphate resulting from ATP hydrolysis (29). This channel is formed by two adjacent protomers (Figure 2-8A). In *Ct*PilB, it involves Arg-436 as well as Arg-293 and Arg-325 in one protomer and Arg-420, Arg-424, His-459 and Arg-469 in the other (Figures 2-1B & 2-8A). The highly reduced ATPase activity of the *Ct*PilB(R436C) variant (Figure 2-8B) is consistent with Arg-436 being part of the channel with critical functions in the ATP hydrolysis cycle.

In the course of this study, it was observed that the steady state kinetics of *Ct*PilB at 37°C is distinct from that at 54°C (Figures 2-5 to 2-7 & S4), the latter being the optimum temperature for this enzyme (Figure 2-4). Figure S4 represents the kinetic profile of *Ct*PilB at 37°C analyzed by the MLG-based and the enzyme-coupled assays, respectively, in the same [ATP] range as in

Figure 2-7A. The incline no longer appeared multiphasic at 37°C. The other noticeable difference

is the ATP concentration at which the rate of the enzyme approaches half V_{max}, which we will refer

to as $K_{0.5}$ for convenience. At 37°C (Figure S4), the $K_{0.5}$ value is near 0.05 mM ATP, which was

the lowest ATP concentration in these experiments. In comparison, the value of $K_{0.5}$ is about 10

times higher at 54°C (Figures 2-5B and 2-7A). These observations are consistent with the well

documented decrease of K_m of Michaelis-Menten enzymes at lower temperature (100). As far as

we are aware, the effect of low temperature on the kinetics of non-Michaelis-Menten enzymes is

yet to be investigated experimentally. It is nevertheless reasonable to assume a profound effect of

temperature on the properties of such an enzyme (101,102). These observations here suggest

caution in the analysis of the enzymatic properties of a protein at a non-optimum temperature.

Conflict of interest: The authors declare that they have no conflict of interest with the contents of this article.

Author contributions: AS performed experiments. AS and ZY designed studies, analyzed data and prepared the manuscript.

Supplementary figures

```
CtPilB   1    M-SAKLGEVLIKEGLITPQQLKEALDYQRA--HGGRLGSILVSLGIVQDEAITAVLSRQYGVPAVNLDLFDVDPNAVRLLPEETARKYMVLPLARNGSTMTLAMVDPANVFAIDDIKPMTGLNIDQVVVSELSLERALARYY-AP//AMQ
MxPilB   1    M-SGRLGELLVRENLISVQQLRKAQEEQQK--NGTRIGTALVKTGAIEESKLTDFLSKQYGVPAINLKDFDVSPDIIKLVPKDVAEKHLVVFVNRAGPSLIVAMCDPSNIFAVDDLKFLTGYNIETVVASEVSIREALERYYaGKGPSLE
GmPilB   1    MQASRLGELLVRNNVITKEQLAKALEEQKSaDGQQRLGSILIKNGLISEPDLTSFLSKQYGGVPSINLSEFEAEQAVVKIIPADVAQKYQIVPVNRAGSTLIIAMADPSNIFAIDDIKFMTGYNVEVVVVASHSAIKAAIDKYY-DQSASLA
PaPilB   1    MNDSIQLSGLSRQLVQANLLDEKTAVQAQAQAQR--NKLSLVTHLVQSKLVSGLALAELSAEQFGIAYCDLNSLDKESFPRDAISEKLVRQHRVIPLWRRGNKLFVGISDPANHQAINDVQFSTGLTTEAILVEDDKLGLAIDKLF-L----SAT
NgPilF   1    -MSVGLLRILVQNQVVTVEQAEHYYNESQA---GKEVLPMLFSDGVISPKSLAALIARVFSYSILLDLRHYPRHRVLMGVLTEQMVEFHCVPVFRRGDKVFFAVSDPTQMPQIQKTVSAAGIAVELVIVEDDQLAGLLDWVG-SRS//LQ
TtPilF   331  PRAKPLGEILVELGLARPEDVEEALQKQRR--GGGRLEDTLVQSGKLRPEALAQAVATQLGYPYVDPEEDPPDGAP LLLPEDLCRRYGVFPHRLEGNRLVLLMKDPRNILALDDVRLA//YEVAPAVATEAAITKLIERFY-GK-----A

CtPilB        EISEALGETDLEVSE--TEED-VLDLSAASADEAPVVKLVNMILVSSLEYGASDIHIEPYEKKFRVRFRVDGLLREVMRPPLKMRAGLTSRIKIMAKLDIAETRLPQDGRIKIKLKRDTGVRDLDFRVSTLPTIWGEKIVLRLLDKEKLMLDMTKLGFEP
MxPilB        DIVGDVG-DDIEVTK--EETE-NIDEMAKAADDAPVVKLVNLILMDAIKKRASDIHVEPYEKKFRVRFRIDGVMYEVVMRPPMKLNAITSRLKIMASLDISERRLPQDGRIKIKMG----GGKRMEFRVSVCPTLFGEKVVMRLLLDKSNLQLDMTKLGFDA
GmPilB        DVMGDLEMDDLEVID--TDDEvDVSSLERATEDAPVVKLVNLILTDAIKRKASDIHIEPYEKFRVRYRIDGVLYEVVMKPPLKLNAITSRIKIMAELDIAERRLPQDGRIKIKLG---GGQDMIYRVSVLPTLFGEKVVLRLLDKSNLQLDMTKLGYPP
PaPilB        DGLAGLDDVDLEGLDiqSADKSTQEDASAEADDAPVVRFVNWMLLDAIKGGSSDLHFEPYRKIYRVRFRTDGMLHFVAKPPIQLASRISARLKVMAGLDISERRKPQDGRIKMRVSKT----KSIDFRVNTLPTLWGEKIVMRILDSSSAQMGIDALGYEE
NgPilF        ELGEGQEEEESHTLYi--DNR--------EAEDGPVPRFIHKTLSDALRSGASDIHFEFYEHNARIRFRVDGQLREVVQPPIAVRGQLASRIKVMSRLDISEKRIPQDGRMQLFPQK--GGKPVDFRVSTLPTLFGEKVVMRILNSDAASLNIDQLGFEP
TtPilF        ELSEIAKEFAKKQAE--EEVE-----SPLELDESAAQKFVKQVIREAFLQDASDIHIEPQNDVQVRLRIDGALREYSTLPKGALNAVISVVKIMGGLNIAEKRLPQDGRVRYREGAI----DVDLRLSTLPTVYGEKAVMRLLKKASDIPEIEDLGFAP

CtPilB        ESLEKFKRQIAKPYGMVLVTGPTGSGKTNTLYSALASLNTPDTNIMTAEDPVEFNLTGINQVQMKFQIGLNFAATLRSFLRQDPNIILVGEICPFETAEIAVKAALTGHLVLSTLHTNDAPSTVSRLMNMGIEFPFLVATSVNLIQAQRLIRRICTECKAP
MxPilB        QPLAWFKEAIDREYGMVLVLTGPTGSGKTTTLYSALSSLNGLDTNICTAEDPVEFNFAGINQVQMHDDIGLNFAAALRSFLRQDPDIIMIGEIRDFETAEIGVKAALTGHLVLSTLHTNDAPGTVSRLLNMGIEFFLVTASLNLIAQKLARRLCFACKKP
GmPilB        DALHYFKEAIHKPFOMVLVTGPTGSGKTVSLYSALGELNKTTENISTAEDPVEFNFAGINQVQMHEDIGLNFAAALRSFLRQDPDIIMIGEIRDFETAEIAIKAALTGHLVLSTLHTNDAPATINRLLNMGVEFPFLVASAVNLITAQRLARRVCSECKQP
PaPilB        DQKELYLAALKQPGQMILVTGPTGSGKTVSLYTGLNILNTTDINISTAEDPVEINLEGINQVNVNPRQGMDFSQALRAFLRQDPDVIMVGEIRDLETAEIAIKAAQTGHMVMSTLHTNSAAETLTRLLNMGVPAFNLATSVNLIIAQRLARKLCSHCKKE
NgPilF        FQKKLLLEAIHREYGMVLVTGPTGSGKTVSLYTCLNILNTRESVNIATAEDPAEINLPGINQVNVNDKQGLTFAAALKSFLRQDPDIIMVGEIRDLETADIAIKAAQTGHMVFSTLHTNNAAPATLSRMLNMGVAPFNIASSVSLIMAQRLLRRLCSCKOE
TtPilF        GVFERFRFKEVISKPYGIFLITGPTGSGKSFTTFSILKRIATPDKNTQTIEDPVEYEIPGINQTQVNPQAGLTFARALRAFLRQDPDIIMVGEIRDSETAKIATEAALTGHLVIATLHTNDAAQAITRLDEMGVEFPTNISAALIGVLSQRLVRRVCEHCKVE

CtPilB        AKIQPPAQTLIELGFTPEEASK-VVIYEGTG//CPKCKGSGYKRVGLYEVMEMNDELRELILIGASALELRKKAIEHGMLTLRRSGLRKIMDGITTIEEVVRETVL  614
MxPilB        AE-NVDEQALIDAGVPEDKIGT-FTMYEKVG--CRDCNDRGYRGRVAIYEVMPFWDGLKELVINGASAAELKQEAIRLGMSSLRMSGLRKMMDGATTLEEVVGNTAP  563
GmPilB        -E-EIPIQALIDAGVSPDEAPS-YVCYKGTG--CVKCNNTGYKGRVGFYQVMPMLEEIRELILNGANTAEIKRESMRLGIKTMRQSGLTKLKEGVTSFEEVLRVTVA  566
PaPilB        HE---VPRETLLHEGPPEDKIGT-FKLYSPVG--CDHCKN-GYKGRVGIYEVVKNTPALQRIIMEEGNSIEIAEQARKEGFNDLRTSGLLKAMQGITSLEEVNRVTKD  566
NgPilF        VE--RPSASALKEVGFTDEDLAKDWKLYGAVG--CDRCRGQGYKGRAGVYEVMPISEEMQRVIMNNGTEVGILDVAYKEGMVDLRRAGILKIMQGITSLEEVTANTND  558
TtPilF        VK--PDPETLRRLGLSEAEIQG-ARLYKGMG--CERCGGTGYKGRYAIHELLVVDDEIRHAIVAGKSATEIKEIARRKGMKTLREDGLYKALQGITTLEEVLARTIE  889
```

|	TtPilF	CtPilB	MxPilB	GmPilB	NgPilF	PaPilB	Average
TtPilF		44.10	41.17	41.64	36.68	37.39	40.20
CtPilB	44.10		60.68	59.07	43.68	43.01	50.11
MxPilB	41.17	60.68		65.72	42.31	45.50	51.08
GmPilB	41.64	59.07	65.72		43.66	45.06	51.03
NgPilF	36.68	43.68	42.31	43.66		50.72	43.41
PaPilB	37.39	43.01	45.50	45.06	50.72		44.34

Figure S1. Alignments (top) and percentage of identity among six T4aP assembly ATPase orthologs. Shown is the alignment of *Ct*PilB with the best studied T4aP PilB orthologs from *Myxococcus xanthus (Mx)*, *Geobacter metallireducens (Gm)*, *Pseudomonas. aeruginosa (Pa)*, *Neisseria gonorrhoeae (Ng)* and *Thermus thermophilus* (*Tt*). The residues are colored by their chemical properties similar as in Figure 2-1B. The rectangle indicates where the N-terminus of *Mx*PilB and C-terminus of *Ct*PilB were fused to produce the chimera that complemented a *pilB* deletion mutation in *M. xanthus* as shown in Figure S2. The table at the bottom right shows the pairwise identity among the amino acids of these orthologs with the average of one with the other five in the last column.
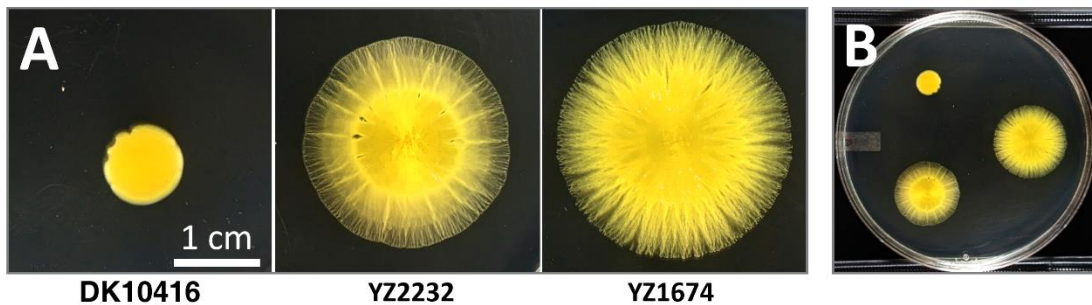

Figure S2. Functionality of a *Mx*PilB-*Ct*PilB chimera in *M. xanthus*. The coding region for the C-terminus of wild-type *Mx*PilB in pWB571 (49) was replaced by that of *Ct*PilB at the junction indicated in Figure S1. The resulting plasmid was transformed into an *M. xanthus pilB* deletion strain DK10416 (Δ*pilB*) to generate YZ2232. T4P-mediated social motility of these strains was analyzed and documented using 0.4% agar plate after 4 days of incubation at 32°C as described previously (49,103). YZ1674, which was constructed by the transformation of DK10416 (Δ*pilB*) with pWB571 (49), was used as the positive control. A 1 cm scale bar is provided for Panel A. Panel B shows the photograph of the petri dish from which the imagines in Panel B originated.
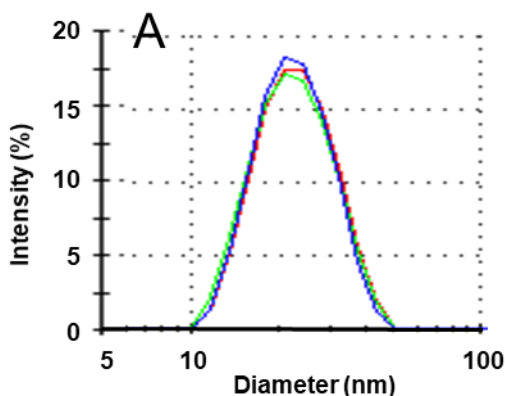
ATP-γ-S (mM)	Diameter (nm)
0	22.29 ± 0.10
0.05	21.97 ± 0.09
0.5	22.42 ± 0.20
1.0	22.46 ± 0.19
1.5	22.75 ± 0.53
3.0	22.84 ± 0.22

Figure S3. Determination of *Ct*PilB particle size by dynamic light scattering (DLS). (A) Samples at 1 mg/ml in gel filtration buffer were incubated at 25°C for 5 minutes before analysis by DLS using a Zetasizer Nano ZS (Malvern Instruments) equipped with a laser at 532 nm wavelength. Data collection and calculations were performed using Zetasizer software v7.11. The settings were for proteins in water as the primary solvent with salts in the buffer accounted for. The hydrodynamic diameter of the particle was calculated according to the Stokes-Einstein equation (104,105). The curves in the three different colors represent the results from three independent measurements, respectively. (B) Samples at 1 mg/ml in activity buffer (see Experimental Procedures) were analyzed with or without ATP-γ-S at 37°C as above and the hydrodynamic diameter of *Ct*PilB similarly calculated. The diameter of *Ct*PilB at different concentrations of ATP-γ-S are calculated from three different measurements with standard deviation indicated.
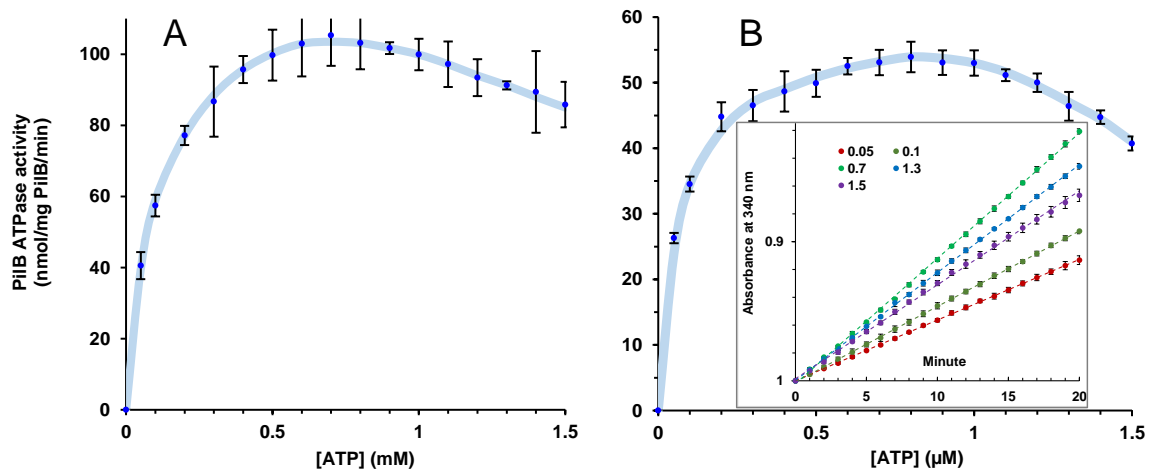
**Figure S4. Comparison of *Ct*PilB ATPase activity by the MLG assay (Panel A) and the enzyme-coupled assay (Panel B) at 37°C.** These experiments were performed using sixteen different ATP concentrations as in Figure 2-7A**.** (A) Experimental results using the MLG assay with rates calculated from time points at 3, 6 and 9 minutes. Preparative experiments indicated that the MLG assay remained linear for at least 30 minutes at 37°C under these condition within the linear range of the standard curve. (B) Results from experiments conducted using the enzyme-coupled assay as described and presented in Figure 2-6B.

CONCLUSIONS

The previous limitation in studying PilB *in vitro* has been overcome by purifying a prototypical PilB from *Chloracidobacterium thermophilum* (*Ct*PilB). *Ct*PilB was successfully purified as a natural hexamer and was demonstrated to exhibit a robust ATPase activity which is significantly higher than any PilB previously studied. The robustness of *Ct*PilB allowed further biochemical studies to elucidate the mechanism of PilB catalysis. Using *Ct*PilB, for the first time the ATPase kinetic profile of an active PilB was studied. The kinetics profile of *Ct*PilB ATPase activity displayed a multiphasic incline and a substrate inhibition decline. The complex kinetics was observed in the physiological ATP range inside the cell indicating that the T4P may be responsive to cellular ATP concentration *in vivo*. This complex kinetic profile is consistent with the model symmetrical rotary mechanism of PilB catalysis supporting the elongated PilB structure. However, further experiments need to be conducted to carefully examine the complex kinetics of PilB and elucidate the mechanism of PilB catalysis. The measured PilB activity in vitro was still lower than the expected activity *in vivo*. This lower activity may suggest the requirement of the other Pil proteins to enhance ATPase PilB activity. Also, *Ct*PilB has provided a solid foundation for further studies on PilB by opening up a new possibility of examining PilB *in vitro*.

REFERENCES

1. Giltner, C. L., Nguyen, Y., and Burrows, L. L. (2012) Type IV pilin proteins: versatile molecular modules. *Microbiology and molecular biology reviews : MMBR* **76**, 740-772
2. Szabo, Z., and Pohlschroder, M. (2012) Diversity and subcellular distribution of archaeal secreted proteins. *Front Microbiol* **3**, 207
3. Ayers, M., Howell, P. L., and Burrows, L. L. (2010) Architecture of the type II secretion and type IV pilus machineries. *Future Microbiology* **5**, 1203-1218
4. McLaughlin, L. S., Haft, R. J., and Forest, K. T. (2012) Structural insights into the Type II secretion nanomachine. *Current opinion in structural biology* **22**, 208-216
5. Kaiser, D. (1979) Social gliding is correlated with the presence of pili in Myxococcus xanthus. *Proc Natl Acad Sci U S A* **76**, 5952-5956
6. Mattick, J. S. (2002) Type IV pili and twitching motility. *Annu Rev Microbiol* **56**, 289-314
7. Craig, L., Pique, M. E., and Tainer, J. A. (2004) Type IV pilus structure and bacterial pathogenicity. *Nat Rev Microbiol* **2**, 363-378
8. Chen, I., and Dubnau, D. (2004) DNA uptake during bacterial transformation. *Nat Rev Microbiol* **2**, 241-249
9. Merz, A. J., So, M., and Sheetz, M. P. (2000) Pilus retraction powers bacterial twitching motility. *Nature* **407**, 98-102
10. Skerker, J. M., and Berg, H. C. (2001) Direct observation of extension and retraction of type IV pili. *Proc Natl Acad Sci USA* **98**, 6901-6904
11. Schuergers, N., Nurnberg, D. J., Wallner, T., Mullineaux, C. W., and Wilde, A. (2015) PilB localisation correlates with the direction of twitching motility in the cyanobacterium Synechocystis sp. PCC 6803. *Microbiology*
12. Clausen, M., Jakovljevic, V., Sogaard-Andersen, L., and Maier, B. (2009) High-force generation is a conserved property of type IV pilus systems. *J Bacteriol* **191**, 4633-4638
13. Maier, B., Potter, L., So, M., Long, C. D., Seifert, H. S., and Sheetz, M. P. (2002) Single pilus motor forces exceed 100 pN. *Proc Natl Acad Sci U S A* **99**, 16012-16017
14. Smith, D. E., Tans, S. J., Smith, S. B., Grimes, S., Anderson, D. L., and Bustamante, C. (2001) The bacteriophage straight phi29 portal motor can package DNA against a large internal force. *Nature* **413**, 748
15. Visscher, K., Schnitzer, M. J., and Block, S. M. (1999) Single kinesin molecules studied with a molecular force clamp. *Nature* **400**, 184-189
16. Wang, M. D., Schnitzer, M. J., Yin, H., Landick, R., Gelles, J., and Block, S. M. (1998) Force and Velocity Measured for Single Molecules of RNA Polymerase. *Science* **282**, 902-907
17. Chang, Y. W., Rettberg, L. A., Treuner-Lange, A., Iwasa, J., Sogaard-Andersen, L., and Jensen, G. J. (2016) Architecture of the type IVa pilus machine. *Science* **351**, aad2001
18. Nunn, D., Bergman, S., and Lory, S. (1990) PRODUCTS OF 3 ACCESSORY GENES, PILB, PILC, AND PILD, ARE REQUIRED FOR BIOGENESIS OF PSEUDOMONAS-AERUGINOSA PILI. *Journal of Bacteriology* **172**, 2911-2919
19. Collins, R. F., Davidsen, L., Derrick, J. P., Ford, R. C., and Tonjum, T. (2001) Analysis of the PilQ secretin from Neisseria meningitidis by transmission electron microscopy reveals a dodecameric quaternary structure. *J Bacteriol* **183**, 3825-3832

20.   Jain, S., Moscicka, K. B., Bos, M. P., Pachulec, E., Stuart, M. C., Keegstra, W., Boekema, E. J., and van der Does, C. (2011) Structural characterization of outer membrane components of the type IV pili system in pathogenic Neisseria. *PloS one* **6**, e16624

21.   Friedrich, C., Bulyha, I., and Sogaard-Andersen, L. (2014) Outside-in assembly pathway of the type IV pilus system in *Myxococcus xanthus*. *J Bacteriol* **196**, 378-390

22.   Jakovljevic, V., Leonardy, S., Hoppert, M., and Sogaard-Andersen, L. (2008) PilB and PilT are ATPases acting antagonistically in type IV pilus function in *Myxococcus xanthus*. *J Bacteriol* **190**, 2411-2421

23.   Mauriello, E. M., Mignot, T., Yang, Z., and Zusman, D. R. (2010) Gliding motility revisited: how do the myxobacteria move without flagella? *Microbiol Mol Biol Rev* **74**, 229-249

24.   Salzer, R., Herzberg, M., Nies, D. H., Joos, F., Rathmann, B., Thielmann, Y., and Averhoff, B. (2014) Zinc and ATP binding of the hexameric AAA-ATPase PilF from Thermus thermophilus: role in complex stability, piliation, adhesion, twitching motility, and natural transformation. *The Journal of biological chemistry* **289**, 30343-30354

25.   Iyer, L. M., Leipe, D. D., Koonin, E. V., and Aravind, L. (2004) Evolutionary history and higher order classification of AAA+ ATPases. *J Struct Biol* **146**, 11-31

26.   Vale, R. D. (2000) AAA proteins. Lords of the ring. *J Cell Biol* **150**, F13-19

27.   Wendler, P., Ciniawsky, S., Kock, M., and Kube, S. (2012) Structure and function of the AAA+ nucleotide binding pocket. *Biochimica et biophysica acta* **1823**, 2-14

28.   Erzberger, J. P., and Berger, J. M. (2006) Evolutionary relationships and structural mechanisms of AAA+ proteins. *Annu Rev Biophys Biomol Struct* **35**, 93-114

29.   Mancl, J. M., Black, W. P., Robinson, H., Yang, Z., and Schubot, F. D. (2016) Crystal Structure of a Type IV Pilus Assembly ATPase: Insights into the Molecular Mechanism of PilB from *Thermus thermophilus*. *Structure* **24**, 1886-1897

30.   McCallum, M., Tammam, S., Khan, A., Burrows, L. L., and Howell, P. L. (2017) The molecular mechanism of the type IVa pilus motors. *Nat Commun* **8**, 15091

31.   Chiang, P., Sampaleanu, L. M., Ayers, M., Pahuta, M., Howell, P. L., and Burrows, L. L. (2008) Functional role of conserved residues in the characteristic secretion NTPase motifs of the Pseudomonas aeruginosa type IV pilus motor proteins PilB, PilT and PilU. *Microbiology* **154**, 114-126

32.   Bischof, L. F., Friedrich, C., Harms, A., Sogaard-Andersen, L., and van der Does, C. (2016) The Type IV Pilus Assembly ATPase PilB of Myxococcus xanthus Interacts with the Inner Membrane Platform Protein PilC and the Nucleotide-binding Protein PilM. *The Journal of biological chemistry* **291**, 6946-6957

33.   Lu, C., Turley, S., Marionni, S. T., Park, Y. J., Lee, K. K., Patrick, M., Shah, R., Sandkvist, M., Bush, M. F., and Hol, W. G. (2013) Hexamers of the type II secretion ATPase GspE from Vibrio cholerae with increased ATPase activity. *Structure* **21**, 1707-1717

34.   Rose, I., Biukovic, G., Aderhold, P., Muller, V., Gruber, G., and Averhoff, B. (2011) Identification and characterization of a unique, zinc-containing transport ATPase essential for natural transformation in Thermus thermophilus HB27. *Extremophiles* **15**, 191-202

35.   Lyubimov, A. Y., Strycharska, M., and Berger, J. M. (2011) The nuts and bolts of ring-translocase structure and mechanism. *Current opinion in structural biology* **21**, 240-248

36. Smith, D. M., Fraga, H., Reis, C., Kafri, G., and Goldberg, A. L. (2011) ATP binds to proteasomal ATPases in pairs with distinct functional effects, implying an ordered reaction cycle. *Cell* **144**, 526-538

37. Craig, L., and Li, J. (2008) Type IV pili: paradoxes in form and function. *Current opinion in structural biology* **18**, 267-277

38. Pelicic, V. (2008) Type IV pili: e pluribus unum? *Mol Microbiol* **68**, 827-837

39. Berry, J. L., and Pelicic, V. (2015) Exceptionally widespread nanomachines composed of type IV pilins: the prokaryotic Swiss Army knives. *FEMS Microbiol Rev* **39**, 134-154

40. Gold, V. A., Salzer, R., Averhoff, B., and Kuhlbrandt, W. (2015) Structure of a type IV pilus machinery in the open and closed state. *Elife* **4**

41. Chang, Y. W., Kjaer, A., Ortega, D. R., Kovacikova, G., Sutherland, J. A., Rettberg, L. A., Taylor, R. K., and Jensen, G. J. (2017) Architecture of the Vibrio cholerae toxin-coregulated pilus machine revealed by electron cryotomography. *Nat Microbiol* **2**, 16269

42. Misic, A. M., Satyshur, K. A., and Forest, K. T. (2010) *P. aeruginosa* PilT structures with and without nucleotide reveal a dynamic type IV pilus retraction motor. *Journal of molecular biology* **400**, 1011-1021

43. Douzi, B., Filloux, A., and Voulhoux, R. (2012) On the path to uncover the bacterial type II secretion system. *Philos Trans R Soc Lond B Biol Sci* **367**, 1059-1072

44. Korotkov, K. V., Sandkvist, M., and Hol, W. G. (2012) The type II secretion system: biogenesis, molecular architecture and mechanism. *Nat Rev Microbiol* **10**, 336-351

45. Bulyha, I., Schmidt, C., Lenz, P., Jakovljevic, V., Hone, A., Maier, B., Hoppert, M., and Sogaard-Andersen, L. (2009) Regulation of the type IV pili molecular machine by dynamic localization of two motor proteins. *Mol Microbiol* **74**, 691-706

46. Carter, T., Buensuceso, R. N., Tammam, S., Lamers, R. P., Harvey, H., Howell, P. L., and Burrows, L. L. (2017) The Type IVa Pilus Machinery Is Recruited to Sites of Future Cell Division. *MBio* **8**

47. Tsai, C. L., and Tainer, J. A. (2016) The ATPase Motor Turns for Type IV Pilus Assembly. *Structure* **24**, 1857-1859

48. Wang, Y. C., Chin, K. H., Tu, Z. L., He, J., Jones, C. J., Sanchez, D. Z., Yildiz, F. H., Galperin, M. Y., and Chou, S. H. (2016) Nucleotide binding by the widespread high-affinity cyclic di-GMP receptor MshEN domain. *Nat Commun* **7**, 1-12

49. Black, W. P., Wang, L., Jing, X., Saldana, R. C., Li, F., Scharf, B. E., Schubot, F. D., and Yang, Z. (2017) The type IV pilus assembly ATPase PilB functions as a signaling protein to regulate exopolysaccharide production in Myxococcus xanthus. *Sci Rep* **7**, 7263

50. Bischof, L. F., Friedrich, C., Harms, A., Sogaard-Andersen, L., and van der Does, C. (2016) The Type IV Pilus Assembly ATPase PilB of *Myxococcus xanthus* interacts with the Inner Membrane Platform Protein PilC and the Nucleotide Binding Protein PilM. *J Biol Chem* **291**, 6946-6957

51. Chiang, P., Sampaleanu, L. M., Ayers, M., Pahuta, M., Howell, P. L., and Burrows, L. L. (2008) Functional role of conserved residues in the characteristic secretion NTPase motifs of the *Pseudomonas aeruginosa* type IV pilus motor proteins PilB, PilT and PilU. *Microbiology (Reading, England)* **154**, 114-126

52. Tank, M., and Bryant, D. A. (2015) Nutrient requirements and growth physiology of the photoheterotrophic Acidobacterium, Chloracidobacterium thermophilum. *Front Microbiol* **6**, 226

53. Bryant, D. A., Costas, A. M., Maresca, J. A., Chew, A. G., Klatt, C. G., Bateson, M. M., Tallon, L. J., Hostetler, J., Nelson, W. C., Heidelberg, J. F., and Ward, D. M. (2007) *Candidatus* Chloracidobacterium thermophilum: an aerobic phototrophic Acidobacterium. *Science* **317**, 523-526

54. Garcia Costas, A. M., Liu, Z., Tomsho, L. P., Schuster, S. C., Ward, D. M., and Bryant, D. A. (2012) Complete genome of *Candidatus* Chloracidobacterium thermophilum, a chlorophyll-based photoheterotroph belonging to the phylum Acidobacteria. *Environ Microbiol* **14**, 177-190

55. Kruse, K., Salzer, R., Joos, F., and Averhoff, B. (2018) Functional dissection of the three N-terminal general secretory pathway domains and the Walker motifs of the traffic ATPase PilF from *Thermus thermophilus*. *Extremophiles* https://doi.org/10.1007/s00792-018-1008-9

56. Bertani, G. (2004) Lysogeny at mid-twentieth century: P1, P2, and other experimental systems. *J Bacteriol* **186**, 595-600

57. Chen, H., Cheng, H., and Bjerknes, M. (1993) One-step Coomassie brilliant blue R-250 staining of proteins in polyacrylamide gel. *Anal Biochem* **212**, 295-296

58. Baykov, A. A., Evtushenko, O. A., and Avaeva, S. M. (1988) A malachite green procedure for orthophosphate determination and its use in alkaline phosphatase-based enzyme immunoassay. *Anal Biochem* **171**, 266-270

59. Leibrock, E., Bayer, P., and Ludemann, H. D. (1995) Nonenzymatic hydrolysis of adenosinetriphosphate (ATP) at high temperatures and high pressures. *Biophys Chem* **54**, 175-180

60. De La Cruz, E. M., and Ostap, E. M. (2009) Kinetic and equilibrium analysis of the myosin ATPase. *Methods Enzymol* **455**, 157-192

61. Kiianitsa, K., Solinger, J. A., and Heyer, W. D. (2003) NADH-coupled microplate photometric assay for kinetic studies of ATP-hydrolyzing enzymes with low and high specific activities. *Analytical biochemistry* **321**, 266-271

62. Biasini, M., Bienert, S., Waterhouse, A., Arnold, K., Studer, G., Schmidt, T., Kiefer, F., Gallo Cassarino, T., Bertoni, M., Bordoli, L., and Schwede, T. (2014) SWISS-MODEL: modelling protein tertiary and quaternary structure using evolutionary information. *Nucleic Acids Res* **42**, W252-258

63. Schrodinger, L. (2010) The PyMOL Molecular Graphics System, Version 1.8 Schrödinger, LLC., New York; 2010

64. Zusman, D. R., Scott, A. E., Yang, Z., and Kirby, J. R. (2007) Chemosensory pathways, motility and development in *Myxococcus xanthus*. *Nat Rev Microbiol* **5**, 862-872

65. Mercier, R., and Mignot, T. (2016) Regulations governing the multicellular lifestyle of *Myxococcus xanthus*. *Curr Opin Microbiol* **34**, 104-110

66. Ciccarelli, F. D., Doerks, T., von Mering, C., Creevey, C. J., Snel, B., and Bork, P. (2006) Toward automatic reconstruction of a highly resolved tree of life. *Science* **311**, 1283-1287

67. Van Veldhoven, P. P., and Mannaerts, G. P. (1987) Inorganic and organic phosphate measurements in the nanomolar range. *Analytical biochemistry* **161**, 45-48

68. Henkel, R. D., VandeBerg, J. L., and Walsh, R. A. (1988) A microassay for ATPase. *Analytical biochemistry* **169**, 312-318

69. Jain, R., Sliusarenko, O., and Kazmierczak, B. I. (2017) Interaction of the cyclic-di-GMP binding protein FimX and the Type 4 pilus assembly ATPase promotes pilus assembly. *PLoS Pathog* **13**, e1006594

70. D'Alessandro, M., Turina, P., and Melandri, B. A. (2011) Quantitative evaluation of the intrinsic uncoupling modulated by ADP and P(i) in the reconstituted ATP synthase of Escherichia coli. *Biochimica et biophysica acta* **1807**, 130-143

71. D'Alessandro, M., Turina, P., Melandri, B. A., and Dunn, S. D. (2017) Modulation of coupling in the Escherichia coli ATP synthase by ADP and Pi: Role of the epsilon subunit C-terminal domain. *Biochimica et biophysica acta* **1858**, 34-44

72. Ferguson, S. A., Cook, G. M., Montgomery, M. G., Leslie, A. G., and Walker, J. E. (2016) Regulation of the thermoalkaliphilic F1-ATPase from Caldalkalibacillus thermarum. *Proc Natl Acad Sci U S A* **113**, 10860-10865

73. Lemkul, J. A., and Bevan, D. R. (2011) Characterization of interactions between PilA from *Pseudomonas aeruginosa* strain K and a model membrane. *J Phys Chem B* **115**, 8004-8008

74. Kubitschek, H. E. (1990) Cell volume increase in Escherichia coli after shifts to richer media. *J Bacteriol* **172**, 94-101

75. Lynch, M., and Marinov, G. K. (2017) Membranes, energetics, and evolution across the prokaryote-eukaryote divide. *Elife* **6**

76. Ueno, H., Suzuki, T., Kinosita, K., Jr., and Yoshida, M. (2005) ATP-driven stepwise rotation of FoF1-ATP synthase. *Proc Natl Acad Sci U S A* **102**, 1333-1338

77. Yamagata, A., and Tainer, J. A. (2007) Hexameric structures of the archaeal secretion ATPase GspE and implications for a universal secretion mechanism. *Embo J* **26**, 878-890

78. Bald, D. (2011) ATP Synthase: Structure, Function and Regulation of a Complex Machine. *Bioenergetic Processes of Cyanobacteria: From Evolutionary Singularity to Ecological Diversity*, 239-261

79. Senior, A. E., Nadanaciva, S., and Weber, J. (2002) The molecular mechanism of ATP synthesis by F1F0-ATP synthase. *Biochim Biophys Acta* **1553**, 188-211

80. Nagar, S., Argikar, U. A., and Tweedie, D. J. (2014) Enzyme kinetics in drug metabolism: fundamentals and applications. *Methods Mol Biol* **1113**, 1-6

81. Marrione, P. E., and Cox, M. M. (1995) RuvB protein-mediated ATP hydrolysis: functional asymmetry in the RuvB hexamer. *Biochemistry* **34**, 9809-9818

82. Marrione, P. E., and Cox, M. M. (1996) Allosteric effects of RuvA protein, ATP, and DNA on RuvB protein-mediated ATP hydrolysis. *Biochemistry* **35**, 11228-11238

83. Huang, H., Zhang, X., Li, S., Liu, N., Lian, W., McDowell, E., Zhou, P., Zhao, C., Guo, H., Zhang, C., Yang, C., Wen, G., Dong, X., Lu, L., Ma, N., Dong, W., Dou, Q. P., Wang, X., and Liu, J. (2010) Physiological levels of ATP negatively regulate proteasome function. *Cell Res* **20**, 1372-1385

84. Monti, J. L. E., Montes, M. R., and Rossi, R. C. (2018) Steady-state analysis of enzymes with non-Michaelis-Menten kinetics: The transport mechanism of Na(+)/K(+)-ATPase. *J Biol Chem* **293**, 1373-1385

85. Kim, Y. C., Snoberger, A., Schupp, J., and Smith, D. M. (2015) ATP binding to neighbouring subunits and intersubunit allosteric coupling underlie proteasomal ATPase function. *Nat Commun* **6**, 8520

86. Bochner, B. R., and Ames, B. N. (1982) Complete analysis of cellular nucleotides by two-dimensional thin layer chromatography. *The Journal of biological chemistry* **257**, 9759-9769

87. Yaginuma, H., Kawai, S., Tabata, K. V., Tomiyama, K., Kakizuka, A., Komatsuzaki, T., Noji, H., and Imamura, H. (2014) Diversity in ATP concentrations in a single bacterial cell population revealed by quantitative single-cell imaging. *Sci Rep* **4**, 6522

88. Buckstein, M. H., He, J., and Rubin, H. (2008) Characterization of nucleotide pools as a function of physiological state in Escherzchia coli. *Journal of Bacteriology* **190**, 718-726

89. Rust, M. J., Golden, S. S., and O'Shea, E. K. (2011) Light-Driven Changes in Energy Metabolism Directly Entrain the Cyanobacterial Circadian Oscillator. *Science* **331**, 220-223

90. Potts, M., and Morrison, N. S. (1986) Shifts in the Intracellular Atp Pools of Immobilized Nostoc Cells (Cyanobacteria) Induced by Water-Stress. *Plant Soil* **90**, 211-221

91. Neuhard, J., and Nygaard, P. (1987) Purines and pyrimidines. in *Escherichia coli and Salmonella typhimurium: cellular and molecular biology* (Neidhardt, F. C. ed.), ASM Press, Washington, D.C. pp 445-473

92. Brovko, L., Romanova, N. A., and Ugarova, N. N. (1994) Bioluminescent assay of bacterial intracellular AMP, ADP, and ATP with the use of a coimmobilized three-enzyme reagent (adenylate kinase, pyruvate kinase, and firefly luciferase). *Analytical biochemistry* **220**, 410-414

93. Alagesan, S., Gaudana, S. B., and Wangikar, P. P. (2016) Rhythmic oscillations in KaiC1 phosphorylation and ATP/ADP ratio in nitrogen-fixing cyanobacterium Cyanothece sp ATCC 51142. *Biol Rhythm Res* **47**, 285-301

94. Schuergers, N., Lenn, T., Kampmann, R., Meissner, M. V., Esteves, T., Temerinac-Ott, M., Korvink, J. G., Lowe, A. R., Mullineaux, C. W., and Wilde, A. (2016) Cyanobacteria use micro-optics to sense light direction. *Elife* **5**

95. Chau, R. M., Ursell, T., Wang, S., Huang, K. C., and Bhaya, D. (2015) Maintenance of motility bias during cyanobacterial phototaxis. *Biophys J* **108**, 1623-1632

96. Schuergers, N., Nurnberg, D. J., Wallner, T., Mullineaux, C. W., and Wilde, A. (2015) PilB localization correlates with the direction of twitching motility in the cyanobacterium Synechocystis sp. PCC 6803. *Microbiology* **161**, 960-966

97. Semmler, A. B., Whitchurch, C. B., and Mattick, J. S. (1999) A re-examination of twitching motility in Pseudomonas aeruginosa. *Microbiology* **145 (Pt 10)**, 2863-2873

98. Hillesland, K. L., and Velicer, G. J. (2005) Resource level affects relative performance of the two motility systems of Myxococcus xanthus. *Microbial ecology* **49**, 558-566

99. Hallenbeck, P. C., Grogger, M., Mraz, M., and Veverka, D. (2016) Draft Genome Sequence of the Photoheterotrophic Chloracidobacterium thermophilum Strain OC1 Found in a Mat at Ojo Caliente. *Genome Announc* **4**

100. Fields, P. A., Dong, Y., Meng, X., and Somero, G. N. (2015) Adaptations of protein structure and function to temperature: there is more than one way to 'skin a cat'. *J Exp Biol* **218**, 1801-1811

101. Maugini, E., Tronelli, D., Bossa, F., and Pascarella, S. (2009) Structural adaptation of the subunit interface of oligomeric thermophilic and hyperthermophilic enzymes. *Comput Biol Chem* **33**, 137-148

102. Gu, J., and Hilser, V. J. (2009) Sequence-based analysis of protein energy landscapes reveals nonuniform thermal adaptation within the proteome. *Mol Biol Evol* **26**, 2217-2227

103. Shi, W., and Zusman, D. R. (1993) The two motility systems of Myxococcus xanthus show different selective advantages on various surfaces. *Proc Natl Acad Sci U S A* **90**, 3378-3382

104. Pecora, R. (2000) Dynamic light scattering measurement of nanometer particles in liquids. *J Nanopart Res* **2**, 123-131

105. Stetefeld, J., McKenna, S. A., and Patel, T. R. (2016) Dynamic light scattering: a practical guide and applications in biomedical sciences. *Biophysical Reviews* **8**, 409-427